Theoretical modeling of heat transfer in vertical upward and downward annular flow boiling

Paul Onubi Ayegba, Julien Sebilleau, Catherine Colin

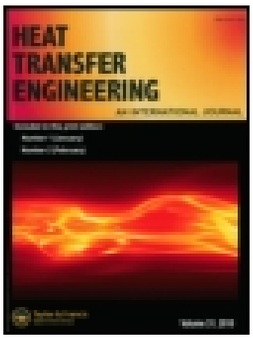

Heat Transfer Engineering

ISSN: (Print) (Online) Journal homepage: https://www.tandfonline.com/loi/uhte20

Theoretical Modelling of Heat Transfer in Vertical Upward and Downward Annular Flow Boiling

Paul Onubi Ayegba, Julien Sebilleau & Catherine Colin

To cite this article: Paul Onubi Ayegba, Julien Sebilleau & Catherine Colin (2023): Theoretical Modelling of Heat Transfer in Vertical Upward and Downward Annular Flow Boiling, Heat Transfer Engineering, DOI: 10.1080/01457632.2023.2191439

To link to this article: https://doi.org/10.1080/01457632.2023.2191439

Accepted author version posted online: 16 Mar 2023.

Theoretical Modelling of Heat Transfer in Vertical Upward and Downward Annular Flow Boiling

Paul Onubi Ayegba, Julien Sebilleau, and Catherine Colin*

Institut de Mécanique des Fluides de Toulouse, Université de Toulouse, Toulouse, France

***CONTACT :** Professor Catherine Colin, Institut de Mécanique des Fluides de Toulouse, Université de Toulouse, CNRS-INPT-UPS Allée Camille Soula, 31400 Toulouse, France. E-mail: catherine.colin@imft.fr

Abstract

This work entails experimental measurement and theoretical modelling of heat transfer coefficient for annular flow boiling in upward and downward flow configurations. The working fluid used was HFE-7000 and experimental measurements were carried out inside a 6 mm sapphire tube coated externally with indium-tin-oxide for Joule heating. The range of vapor quality, mass flux and heat flux investigated were 0.15 – 0.7, 75 – 400 kg/(m^2s) and 0.5 – 3.0 W/cm^2 respectively. Theoretical models for predicting heat transfer coefficient in upward and downward flows were developed using heat-flux-dependent wall shear stress correlations and roll-wave-velocity-based interfacial damping function. It was found that interfacial damping depends on the Reynolds number of the liquid film. The proposed models predicted over 96% of the measured heat transfer coefficient within ± 20% in both upward and downward flows and reproduced the heat flux

dependence of the heat transfer coefficient. The models also predicted over 96% of the measured liquid film thickness within ± 30% in both upward and downward flows.

Introduction

Flow boiling is encountered in various applications such as in the production of electricity in nuclear power plants, energy conservation and process industries. Flow boiling thermal systems take advantage of the latent heat in phase change. Modelling studies of phase change heat transfer have mainly focused on semi-empirical correlations [1–7] and algebraic eddy viscosity models by [8–10]. Such models are generally valid for specific flow configurations and relatively narrow ranges of operating conditions. Theoretical modelling approaches are generally more robust and provide heat transfer predictions over a wider range of operating conditions [11]. Theoretical models also provide a better representation of the physics of the flow.

A common theoretical approach entails the prediction of heat transfer coefficient (*HTC*) from turbulent eddy diffusivity in the liquid film of annular flow. This modelling approach requires, among other things, closure law for interfacial shear stress (τ_i) or wall shear stress (τ_w) (for control volume analyses adjacent to the interface or adjacent to the wall respectively). The interfacial shear stress or wall shear stress is usually obtained from suitable correlations [12]. In the current work, control volume analysis was done adjacent to the wall in other to capture the effect of bubble nucleation at the wall on the wall shear stress and on the eddy viscosity and diffusivity. Most of the existing correlations for two-phase wall shear stress are applicable to adiabatic two-phase flows and in the convective dominant regime of flow boiling [13, 14]. When there is significant nucleation in the annular film, wall shear stress differs quite remarkably from adiabatic two-phase flows [15–18].

Bubble nucleation at the heated wall in flow boiling alters the velocity profile close to the wall which in turn modifies the wall shear stress and heat transfer. Nucleation in the annular film increases fluid mixing inside the film which alters the Prandtl mixing length. It is, therefore, important to use relevant modelling of wall shear stress in flow boiling to develop heat transfer models.

In theoretical modelling of eddy viscosity, it is also important to account for turbulent damping close to wall as well as damping close to the interface [12, 19]. The eddy viscosity (ε_m) from Prandtl mixing length theory is given by:

$$\frac{\varepsilon_m}{v_l} = l^{+2}\frac{du^+}{dy^+} \tag{1}$$

$$l^+ = Ky^+ \tag{2}$$

$$y^+ = \frac{y}{y*},\ u^+ = \frac{u_l}{u^*},\ l^+ = \frac{l}{y^*},\ y^* = \frac{\mu_l}{\rho_l \times u^*} \text{ and } u^* = \sqrt{\frac{\tau_w}{\rho_l}}, \tag{3}$$

where μ_l is the liquid kinematic viscosity, u_l the local liquid velocity in the film, ρ_l the liquid density, l^+ is the dimensionless mixing length, $K = 0.41$ is the von Karman constant, y^+ is the dimensionless distance from the wall, τ_w is the wall shear stress and u^* the friction velocity. To account for wall damping, Van Driest [20] proposed a modification to the dimensionless mixing length given by:

$$l^+ = K\,y^+\left[1 - exp\left(-\sqrt{\frac{\tau}{\tau_w}}\frac{y^+}{A^+}\right)\right] \tag{4}$$

where the term in the square bracket is referred to as the Van Driest wall damping function. $A^+$is a constant and was given equal to 26 by Van Driest [20]. Kays [21] and Kays and Crawford [22]

proposed an expression for A^+ which has found more general application [12, 19, 23–25] and is given by:

$$A^+ = 26{X_{lam}}^{-1} \qquad \left\{X_{lam} = 1 + 30.18\left[\frac{\mu_l\left(\frac{dp}{dz}\right)}{\rho_l^{0.5}\tau_w^{1.5}}\right]\right\} \tag{5}$$

X_{lam} is the laminarization parameter which accounts for the effect of free stream pressure gradient (dp/dz) on the Van Driest [20] damping function.

To account for interfacial damping of turbulent eddies due to the action of surface tension, Mudawwar and El-Masri [19] and other recent studies proposed the introduction an interfacial damping function (Eq. (6)) to the expression for eddy viscosity, δ^+ being the dimensionless liquid film thickness and *n* constant.

$$(1 - y^+/\delta^+)^n \text{ (Interfacial damping function)} \tag{6}$$

The surface tension damping at the interface has been linked to the suppression of small waves or ripples at the interface [19]. In general, increase in surface density and/or amplitude of small waves at the interfaces results in reduced interfacial damping [19]. The converse the case with roll waves because increase velocity and frequency of roll waves results in decreased in small waves. The value of the exponent n in the following studies are 1.0 [19], 0.1 [4, 12, 24] and 0 [20, 23]. In these works, the value of n used was that which gave best prediction of the measured heat transfer coefficient. A small value of n (e.g., $n = 0.1$) means significant mixing or turbulence intensity close to the interface while a high value of n (e.g., 1.0) signifies significant turbulence damping or flow laminarization close to the interface. Because velocity profile in the liquid film close to the interface is significantly influenced by interfacial wave structures, the choice of a constant value of n would at best provide an estimated mean value. Furthermore, when there is nucleation in the

annular film, bubble growth and coalescence with the interface may result in interfacial disturbances. It is therefore important to determine suitable values of n based on wave structures and/or other relevant flow parameters. In this work, theoretical modelling of heat transfer in upward and downward annular flows was done using suitable modelling of the wall shear stress, eddy viscosity profile in the liquid film including damping at the interface.

In the next section the experimental set-up and measurements technics for the study of flow boiling in millimetric tubes in vertical and downward flow are briefly described. The experimental results have been extensively reported in the paper of Ayegba et al. [17] and will be used in this work for the validation of the models. The third session of the manuscript is devoted to the presentation of the theoretical model and the last session to the comparison of the model with the experimental data.

Experimental Setup and Data Reduction

Experimental setup

A detailed description of the experimental setup used for this work is available in [17]. Figure 1 is a schematic drawing of the hydraulic loop used in the current work. The experimental fluid used was 1-methoxyheptafluoropropane ($C_3F_7OCH_3$) refrigerant, commonly called HFE-7000 which has a saturation temperature (T_{sat}) of $34^oC\ at\ 1\ bar$. The fluid temperature at the inlet of the preheater was set at $T_{sat} - 10^oC$. Two-phase vapor-liquid flow was generated in a series of preheaters and passes through a 22 cm long vertical adiabatic section before entering the test section. The pressure at the inlet of the test section was between 1.2 to 1.5 bar. The test section consisted of a vertical transparent sapphire tube of 0.6 $cmID$, 20 cm long and 0.1 cm thick, coated externally with indium-tin-oxide (ITO) for Joule heating. The coating was transparent allowing flow

visualization. Vapor quality at the outlet of the test section was determined by enthalpy balance along the test section and was in the range of $0.15 \leq x \leq 0.70$. The two-phase flow at the outlet of the test section was condensed and cooled to the desired temperature at the inlet of the pump using two PID-controlled Peltier modules in the condenser. The ranges of mass and heat flux tested were $75 \leq G \leq 400\ kg/(m^2 s)$ and $0.5 \leq q \leq 3.0\ W/cm^2$ respectively. This experimental set-up allowed the determination of void fraction and heat transfer coefficient in upward and downward vertical flow configurations. Analysis of images obtained from high-speed visualization was also used in this work to describe the interfacial wave structures. Measurement instrumentations used included Coriolis flow meter, absolute pressure transmitters (Keller PAA21), thermocouples (K- and T-type), PT100 temperature probes, void fraction probes (capacitance type) and a high-speed camera (PCO Dimax). Description of the test section along with measurement uncertainties are available in a previous publication [17].

Data reduction

In the annular flow regime, the fluid at the inlet of the test section was at saturated conditions. The vapor quality at the inlet of the test section (x_{in}) was determined from the enthalpy balance across the preheater and adiabatic section (insulated stainless steel and flexible tube) upstream of the test section (Eq. (7)).

$$\frac{P_{ph\_eff}}{(\pi D^2/4)} = G(1 - x_{in})Cp_l T_{in} + G x_{in} h_v - G Cp_l T_{in,ph} \quad (7)$$

T_{in} and x_{in} are the temperature and the vapor quality at the inlet of the test section, $T_{in,ph}$ is the temperature at the inlet of the preheater, P_{ph_eff} is the preheater power after correction for heat losses, which is the effective power transmitted to the fluid, G is the total mass flux, h_v is the

enthalpy of the vapor and Cp_l is the specific heat capacity of the liquid. For saturated conditions at the inlet of the test section.

$$Cp_l T_{in} = h_{l,sat}\ ,\ h_v = \ h_{v,sat}\ and\ \ h_{v,sat} - h_{l,sat} = h_{lv} \tag{8}$$

$$x_{in} = \frac{4P_{ph\_eff} - GCp_l\pi D^2\left(T_{in} - T_{in,ph}\right)}{G\pi D^2 h_{lv}} \tag{9}$$

were $h_{l,sat}$ and $h_{v,sat}$ are the enthalpy of liquid and vapor at saturation.

The vapor quality (x_z) at an axial position (z) in the test section was obtained from the enthalpy balance between the inlet of the test section and the position z.

$$x_z = x_{in} + \frac{4q_{eff} \times z}{GDh_{lv}} \tag{10}$$

The effective wall heat flux (q_{eff}) was obtained by subtracting the heat loss in the test section from the applied heat flux (q).

Calculation of inner wall heat transfer coefficient (h_i) was done at 4 axial locations along the test section [17]. The heat transfer coefficient at the inner wall was obtained from an energy balance between the fluid and the inner wall as follows:

$$h_i = \frac{q_{eff}}{T_{ow} - T_{i\infty} - ln\left(\frac{R_o}{R_i}\right)\frac{R_o}{k}q_{eff}} \tag{11}$$

where k is the thermal conductivity of sapphire tube, R_o and R_i are the outer and inner tube radii of the sapphire tube, T_{ow} and $T_{i\infty}$ are the outer wall temperature and the liquid bulk temperature.

The capacitance probes have been used to measure the void fraction α at the inlet and outlet

of the test section. In annular flow the liquid film thickness δ is related to the measured value of the fraction α [26].

$$\delta = 0.5D\left(1 - \sqrt{\alpha}\right) \tag{12}$$

For the mass fluxes limited to $400\,kg/(m^2 s)$ the entrainment rate of the droplet estimated using the model of Cioncolini et al. [27] can be neglected in the evaluation of the film thickness [17, 26]. The wall and interfacial shear stresses in annular flow have been derived from combined measurement of the pressure drop along the test section and void fraction.

The uncertainties in the measured vapor quality, mass flux, heat flux, liquid film thickness and heat transfer coefficient are provided in [17]. The measurements of the heat transfer coefficients, wall shear stress and film thickness will be used for the validation of the theoretical model.

Theoretical Modelling of Eddy Viscosity and Eddy Diffusivity

Model assumptions

The local equations for mass, momentum and energy conservation in the liquid film will be derived under the following assumptions and integrated other a control volume (Figure 2):

1. The flow is co-current, at steady state and the liquid is incompressible.
2. The pressure is uniform in the tube cross section.
3. The flow is axisymmetric and the averaged liquid film thickness δ is uniform around the circumference of the tube.

4. Thermo-physical properties of the phases are assumed constant and taken at saturation temperature.

5. The liquid film is supposed to be single-phase flow: interfacial mass and momentum transfer are neglected in the liquid film, except at the interface with the vapor core. The effect of the bubble nucleation is only considered in the modification of the wall shear stress.

6. Entrained liquid fraction in the vapor core is neglected [17, 26].

7. Axial momentum changes in the liquid film are negligible [28].

Eddy viscosity modelling

The momentum balance equation for the liquid phase in the axial direction (Figure 2) is given as:

$$\frac{1}{r}\frac{\partial}{\partial r}(r\tau) + \frac{dp}{dz} + \rho_l g\, sin\,\theta + \frac{d}{dz}(\rho_l {u_l}^2) = 0 \tag{13}$$

$$[u_l]_z = [u_l(r)]_z \tag{14}$$

Integrating Eq. (13) across the liquid film (from r to R) and assuming negligible acceleration in the liquid film gives:

$$\tau = \tau_w \frac{R}{r} + \frac{(R^2 - r^2)}{2r}\left(\frac{dp}{dz} + \rho_l g\, sin\,\theta\right) \tag{15}$$

where τ and τ_w are the shear stresses in the liquid film and tube wall respectively, r and R are the radial distances of the control volume and wall respectively, p is the pressure and θ is the inclination from the horizontal [28]. The second term in the bracket accounts is the hydrostatic pressure gradient and is zero of horizonal and microgravity flows.

In terms of the distance from the wall, Eq. (15) becomes:

$$\tau = \tau_w \frac{R}{(R-y)} + \frac{y(2R-y)}{2(R-y)}\left(\frac{dp}{dz} + \rho_l g \sin\theta\right) \qquad (y = R - r) \tag{16}$$

And in dimensionless form Eq. (16) can be written:

$$\frac{\tau}{\tau_w} = \frac{R^+}{(R^+ - y^+)} + \frac{y^+(2R^+ - y^+)}{2(R^+ - y^+)}\left(\frac{y^{*2}}{\mu_l \times u^*}\right)\left(\frac{dp}{dz} + \rho_l g \sin\theta\right) \tag{17}$$

For turbulent liquid films:

$$\tau = -\mu_l\left(1 + \frac{\varepsilon_m}{v_l}\right)\frac{du_l}{dr} = \mu_l\left(1 + \frac{\varepsilon_m}{v_l}\right)\frac{du_l}{dy} \qquad (r = R - y,\ dr = -dy) \tag{18}$$

where ε_m is the eddy viscosity, μ_l is the dynamic viscosity of the liquid, u_l is the velocity of the liquid which is dependent of the distance (y) from the tube wall. In dimensionless form Eq. (18) is written as:

$$\frac{\tau}{\tau_w} = \left(1 + \frac{\varepsilon_m}{v_l}\right)\frac{du^+}{dy^+} \tag{19}$$

Integrating Eq. (19) from 0 to y^+ gives the velocity profile (u^+) in the liquid film as follows:

$$u_l^+(y^+) = \int_0^{y^+} \frac{\tau}{\tau_w}\left(1 + \frac{\varepsilon_m}{v_l}\right)^{-1} dy^+ \tag{20}$$

For known values of total mass flux G, wall heat flux $q_w\,(q_{eff})$, vapor quality x and fluid properties, the velocity profile in the liquid film can be determined from Eq. (20), if relations for $dp/dz\,, \tau_w, \varepsilon_m/v_l$ and the liquid film thickness δ are available simultaneously.

dp/dz in Eqs. (15-17) may be derived from the momentum balance of the two-phase mixture:

$$\frac{dp}{dz} = -\frac{2}{R}\tau_w - \rho_m g\, sin\,\theta - G^2 \frac{d}{dz}\left[\frac{(1-x)^2}{\rho_l(1-\alpha)} + \frac{x^2}{\rho_v \alpha}\right] \tag{21}$$

where α is the void fraction ($\alpha \approx r_i^2/R^2 \approx (R-\delta)^2/R^2$), r_i is the distance between the tube centre and the interface and

$$\rho_m = \rho_l(1-\alpha) + \rho_v \alpha \tag{22}$$

The second term in the right-hand-side is the gravitational term and the third term is the acceleration term which for constant density yields:

$$G^2 \frac{d}{dz}\left[\frac{(1-x)^2}{\rho_l(1-\alpha)} + \frac{x^2}{\rho_v \alpha}\right] = G^2 \frac{dx}{dz}\left\{\left[\frac{2x}{\rho_v \alpha} - \frac{2(1-x)}{\rho_l(1-\alpha)}\right] + \frac{d\alpha}{dx}\left[\frac{(1-x)^2}{\rho_l(1-\alpha)^2} - \frac{x^2}{\rho_v \alpha^2}\right]\right\} \tag{23}$$

Therefore Eq. (21) becomes:

$$\frac{dp}{dz} = -\frac{2}{R}\tau_w - \rho_m g\, sin\,\theta - G^2 \frac{dx}{dz}\left\{\left[\frac{2x}{\rho_v \alpha} - \frac{2(1-x)}{\rho_l(1-\alpha)}\right] + \frac{d\alpha}{dx}\left[\frac{(1-x)^2}{\rho_l(1-\alpha)^2} - \frac{x^2}{\rho_v \alpha^2}\right]\right\} \tag{24}$$

where

$$\frac{dx}{dz} = \frac{2}{R}\frac{q}{G h_{lv}} \text{ (valid for saturated boiling)} \tag{25}$$

h_{lv} is latent heat and $\frac{d\alpha}{dx}$ is estimated from the drift flux model [17] and given by:

$$\alpha = \frac{Gx/\rho_v}{C_0[Gx/\rho_v + G(1-x)/\rho_l] + u_\infty} \qquad (C_0 \approx 1.2, u_\infty \approx \pm 0.15\ m/s) \tag{26}$$

$$\frac{d\alpha}{dx} = \frac{G}{\rho_v[C_0\, Gx/\rho_v + C_0 G(1-x)/\rho_l + u_\infty]} - \frac{Gx(C_0\, G/\rho_v - C_0 G/\rho_l)}{\rho_v[C_0\, Gx/\rho_v + C_0 G(1-x)/\rho_l + u_\infty]^2} \tag{27}$$

As discussed in the introduction, the wall shear stress (τ_w) in Eq. (24) may be obtained from

suitable correlations. It was also highlighted in the Introduction that the wall shear stress is influenced by wall heating. Wall shear stress is generally higher in flow boiling than adiabatic two-phase flows and the difference increases with wall heat flux [15–17]. Due to the foregoing, Kim and Mudawar [16] proposed a correlation for predicting upward flow boiling wall shear stress by modifying the model for adiabatic two-phase flow proposed by Kim and Mudawar [29]. The model highlighted the heat flux dependence of the wall shear stress. Examination of the model by Ayegba et al. [17], showed some limitations of the model in both the convective and nucleate boiling dominant regimes. Furthermore, the model of Kim and Mudawar [16] was limited to upward flow. Ayegba et al. [17], proposed modifications to the expressions for C_A and C_{NA} in the model of Kim and Mudawar [16] to provide better prediction of the wall shear stress in both upward and downward boiling flows (Eqs. (28-34). The modified correlations were used for the determination of τ_w in the current work and are valid for $1 \leq p \leq 2\ bar$, $75 \leq G \leq 200\ kg/(m^2 s)$, $0 \leq q \leq 3\ W/cm^2$, $0.05 \leq x \leq 0.8$ and $D = 6\ mm$. A comparison of model predictions with experimental data of Ayegba et al. [17] is shown in Figure 3 for reference purpose. The model predicted over 96% of the measured data within $\pm 15\%$ and also captured the effect of heat flux on wall shear stress.

$$\left(\frac{dp}{dz}\right)_{fr} = \frac{4\tau_{w\_2\emptyset}}{D} = \emptyset_l^2 \left(\frac{dp}{dz}\right)_l \tag{28}$$

$$\emptyset_l^2 = 1 + \frac{C_{NA}}{X} + \frac{1}{X^2} \tag{29}$$

$$X = \left[\left(\frac{dp}{dz}\right)_l \Big/ \left(\frac{dp}{dz}\right)_v\right]^{0.5} \tag{30}$$

$$\left(\frac{dp}{dz}\right)_l = -\frac{4}{D} f_l \frac{\rho_l j_l^2}{2} = -f_l \frac{2G^2(1-x)^2}{\rho_l D} \tag{31}$$

$$\left(\frac{dp}{dz}\right)_v = -\frac{4}{D} f_v \frac{\rho_v j_v^2}{2} = -f_v \frac{2G^2 x^2}{\rho_v D} \tag{32}$$

$$C_A = \begin{cases} 0.33 Re_{lo}^{0.03} Su_{vo}^{0.1} (\rho_l/\rho_v)^{0.35} (1/X^{0.22}), & Re_l \geq 3000, Re_v \geq 3000 \\ 0.40 Re_{lo}^{0.03} Su_{vo}^{0.1} (\rho_l/\rho_v)^{0.35} (1/X^{0.27}), & Re_l < 3000, Re_v \geq 3000 \end{cases} \tag{33}$$

$$C_{NA} = \begin{cases} C_A[1 + 30 We_l^{0.32} Bo^{0.78}] & Re_l \geq 1500 \\ C_A[1 + 320 We_{lo}^{0.52} Bo^{1.09}] & Re_l < 1500 \end{cases} \tag{34}$$

$$C_A = \begin{cases} 0.38 Re_{lo}^{0.03} Su_{vo}^{0.1} (\rho_l/\rho_v)^{0.35} (1/X^{0.22}), & Re_l \geq 3000, Re_v \geq 3000 \\ 0.47 Re_{lo}^{0.03} Su_{vo}^{0.1} (\rho_l/\rho_v)^{0.35} (1/X^{0.30}), & Re_l < 3000, Re_v \geq 3000 \end{cases} \tag{35}$$

$$C_{NA} = \begin{cases} C_A[1 + 30 We_l^{0.32} Bo^{0.78}] & Re_l \geq 1500 \\ C_A[1 + 400 We_{lo}^{0.52} Bo^{1.09}] & Re_l < 1500 \end{cases} \tag{36}$$

$$f_k = \begin{cases} 16 Re_k^{-1} & Re_k < 1500 \\ 0.079 Re_k^{-0.25} & 1500 \leq Re_k < 20000 \\ 0.046 Re_k^{-0.2} & Re_k \geq 20000 \end{cases} \tag{37}$$

where k stands for liquid (l) or vapor (v),

$$Re_l = \frac{G(1-x)D}{\mu_l}, Re_{lo} = \frac{GD}{\mu_l}, Re_v = \frac{GxD}{\mu_v}, Re_{vo} = \frac{GD}{\mu_v}, Su_{vo} = \frac{\rho_v \sigma D}{\mu_v^2} \tag{38}$$

$$We_l = \frac{G^2(1-x)^2 D}{\rho_l \sigma}, We_{lo} = \frac{G^2 D}{\rho_l \sigma}, Bo = \frac{q}{G h_{lv}} \tag{39}$$

Several algebraic eddy diffusivities expressions have also been proposed to obtain the velocity profile u_l^+ in the liquid film (Eq. (20)). Simple expressions as constant eddy viscosity [8, 9] or quadratic expression [10] were proposed and led to an analytical expression of heat transfer

coefficient. However, these models do not provide a realistic shape of the velocity and temperature profiles in the liquid film and were not able to reproduce the effect of the heat flux on the heat transfer coefficient [17]. Therefore, we decided to base our analysis on the models proposed by Kim and Mudawar [12] and Mudawar and El-Masri [19].

Substituting Eqs. (4) and (19) into Eq. (1) gives the following expression for eddy viscosity:

$$\frac{\varepsilon_m}{v_l} = -\frac{1}{2} + \frac{1}{2}\sqrt{1 + 4K^2 y^{+2}\left[1 - exp\left(-\sqrt{\frac{\tau}{\tau_w}}\frac{y^+}{A^+}\right)\right]^2 \frac{\tau}{\tau_w}} \tag{40}$$

To account for interfacial damping, Mudawar and El-Masri [19] introduced an interfacial damping function Eq. (6) to the expression for turbulent eddy diffusivity (Eq. (40)) resulting in:

$$\frac{\varepsilon_m}{v_l} = -\frac{1}{2} + \frac{1}{2}\sqrt{1 + 4K^2 y^{+2}\left[1 - exp\left(-\sqrt{\frac{\tau}{\tau_w}}\frac{y^+}{A^+}\right)\right]^2 \frac{\tau}{\tau_w}\left(1 - \frac{y^+}{\delta^+}\right)^n} \tag{41}$$

δ^+ is the dimensionless liquid film thickness and n is an empirical constant.

The remaining parameter for closure of Eq. (20) is the liquid film thickness (δ). This is accomplished using a numerical scheme involving a guess value of δ and relevant boundary conditions. For mass conservation in the liquid film, it is required that the mass flow rate of the liquid film be

$$\dot{m}_l = (1-x)\dot{m} = (1-x)G\pi R^2 = 2\pi\rho_l \int_0^{\delta} (R-y) \times u_l dy = 2\pi\rho_l \int_r^R r \times u_l dr \tag{42}$$

where $\dot{m}$ is the total mass flow rate. Eq. (42) is used to determine if the guess value of δ satisfies

the mass conservation in the liquid film. It should be remarked that in the current work, the liquid entrainment had negligible effect on the liquid film thickness [17, 26] and is not considered in Eq. (42).

Eddy heat diffusivity modelling

The energy balance equation in the annular film writes:

$$\frac{1}{r}\frac{\partial}{\partial r}(rq) = 0 \tag{43}$$

where q is the local diffusive and turbulent heat flux heat, expressed using Boussinesq the assumption:

$$q = (k_l + k_t)\frac{dT}{dr} = -(k_l + k_t)\frac{dT}{dy} = -k_l\left(1 + \frac{k_t}{k_l}\right)\frac{dT}{dy} = -k_l\left(1 + \frac{Pr_l}{Pr_t}\frac{\varepsilon_m}{v_l}\right)\frac{dT}{dy} \tag{44}$$

$$Pr_l = \frac{Cp_l\mu_l}{k_l},\ \ Pr_t = \frac{Cp_l\mu_t}{k_t},\ \ \frac{k_t}{k_l} = \frac{Pr_l}{Pr_t}\frac{\mu_t}{\mu_l} = \frac{Pr_l}{Pr_t}\frac{\varepsilon_m}{v_l} \tag{45}$$

where Cp_l is the specific heat capacity of the liquid, k_l and k_t are liquid and turbulent thermal conductivities, Pr_l and Pr_t are liquid and turbulent Prandtl numbers. Integrating Eq. (43) yields:

$$q/q_w = R/(R - y) \tag{46}$$

The dimensionless temperature in the liquid film is defined as:

$$T^+ = \rho_l Cp_l u^*(T_w - T)/q_w \tag{47}$$

In dimensionless form, Eq. (44) is given by:

$$\frac{q}{q_w} = \frac{1}{Pr_l}\left(1 + \frac{Pr_l}{Pr_t}\frac{\varepsilon_m}{v_l}\right)\frac{dT^+}{dy^+} \tag{48}$$

where

$$dT = -(q_w/\rho_l Cp_l u^*)dT^+,\ dy = -(\mu_l/\rho_l u^*)dy^+ \tag{49}$$

T_w is the wall temperature. The turbulent Prandtl number was given by Mudawar and El-Masri [19] as:

$$Pr_t = 1.4exp(-15\,y^+/\delta^+) + 0.66 \tag{50}$$

Integrating Eq. (47) from 0 to δ^+ and Eq. (48) from 0 to y^+ give the heat transfer coefficient (Eq. (51)) and the dimensionless temperature profile (Eq. (52)) respectively.

$$h = \frac{q_w}{T_w - T_{sat}} = \frac{\rho_l Cp_l u^*}{T_\delta^+} = \frac{\rho_l Cp_l u^*}{\int_0^{\delta^+} \frac{q}{q_w}\left[\frac{1}{Pr_l}\left(1 + \frac{Pr_l}{Pr_t}\frac{\varepsilon_m}{v_l}\right)\right]^{-1} dy^+} \tag{51}$$

$$T^+ = \int_0^{y^+} \frac{q}{q_w}\left[\frac{1}{Pr_l}\left(1 + \frac{Pr_l}{Pr_t}\frac{\varepsilon_m}{v_l}\right)\right]^{-1} dy^+ \tag{52}$$

Solution algorithm and model validity range

The algorithm for the resolution of the equations is depicted in Figure 4 and the numerical simulation was done using MATLAB programming. Turbulent eddy diffusivity models are generally valid for the turbulent flows. In single-phase flow in a pipe the transition from laminar to turbulent occurs for a *Re* number around 2000. In liquid film in annular flow, the momentum and heat diffusivity are enhanced due to the high shear at the interface and in flow boiling due to bubble nucleation at the wall which induces a significant mixing. In the works of Kim and Mudawar [11, 12], eddy diffusivity model was applied to flow boiling in mini/micro channels for $10 \leq$

$Re_l(\overline{u_l}, \delta) \leq 600, Re_l(\overline{u_l}, \delta)$ being the Reynolds number based on the mean liquid velocity in the film and the film thickness. In the current work, the range of liquid film Reynolds number was $700 \leq Re_l(\overline{u_l}, \delta) \leq 6500$.

Results

In this section, results of upward flow are presented first followed by results for downward flow. For each flow orientation, the results of eddy viscosity, liquid velocity and liquid temperature profiles are discussed for two values of n. This is followed by comparison between predicted and measured heat transfer coefficient. Afterwards, an expression for determining suitable values of n is proposed with the aim of improving heat transfer prediction. Model predictions using this n-function is then discussed. Finally, results of predicted and measured liquid film thickness is discussed.

Heat transfer coefficient in upward flow

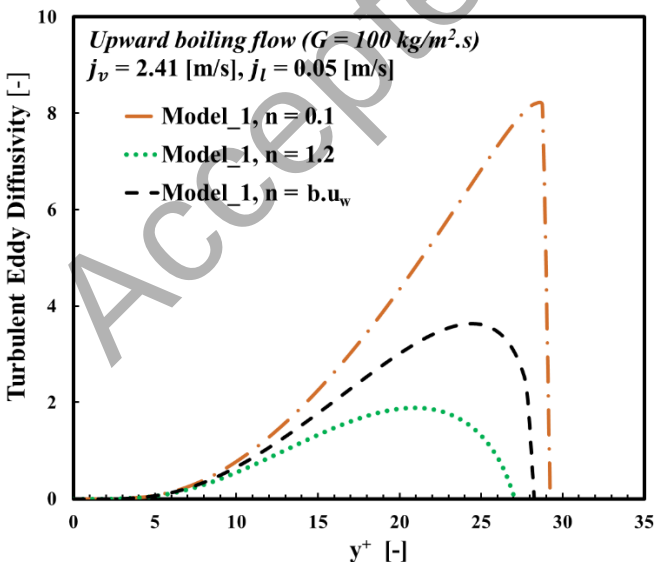

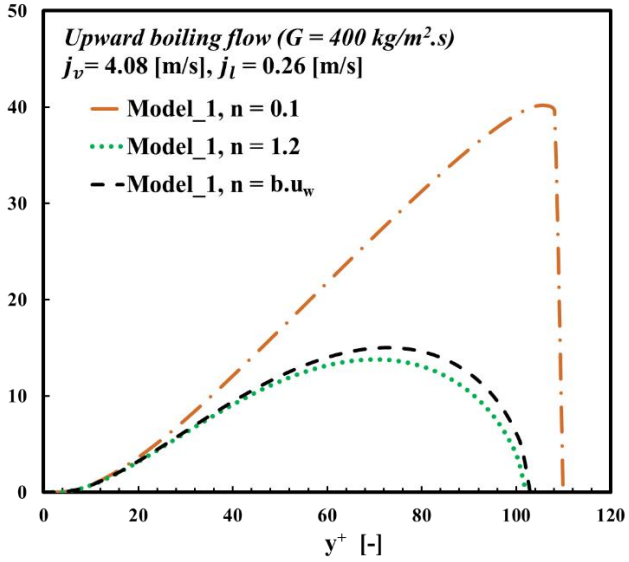

Figure *5* shows eddy viscosity profiles as a function of dimensionless distance from the wall, for two constant values of n (0.1 and 1.2) and a value of n ($b.u_w$) that is linked to the roll wave velocity. It should be remarked that, with change in the value of n, the film thickness at which mass conservation in the liquid film is obtained changes (maximum value of y^+). With increase in n, there is increase in the thickness of the damped layer close to the interface and a lower value of the eddy viscosity in the liquid film. Figure 6 shows predicted velocity and temperature profiles in the liquid film at selected flowrates as a function of dimensionless distance from the wall. With increasing value of n, the dimensionless velocity and temperature profiles increased, and the results agree with similar works in literature [11, 25, 30]. Experimental measurements of the velocity profiles in the annular liquid film have been carried out for adiabatic gas-liquid flows [31, 32]. Similar to the current work, the measured dimensionless velocity and temperature profiles were higher than single phase flow and increased with n. Experimental measurements close to the interface has not been very successful due to limitations of common diagnostics. However, the limited experimental data available also showed changes in the velocity profile as the interface is approached [31, 32].

Figure 7 and Figure *8* provide comparisons between predicted (Eq. (51)) and measured values of heat transfer coefficient in upward flow. For a n value of 0.1, the model generally over-predicts the measured heat transfer for $G = 200\,kg/(m^2s)$ $(1700 \leq Re_l(\overline{u_l}, \delta) \leq 3000)$ and $G = 400\,kg/(m^2s)$ $(4600 \leq Re_l(\overline{u_l}, \delta) \leq 6500)$. Although it also over-predicts the measured heat transfer for $G = 75\,kg/(m^2s)$ $(700 \leq Re_l(\overline{u_l}, \delta) \leq 1000)$ and $G = 100\,kg/(m^2s)$ $(800 \leq Re_l(\overline{u_l}, \delta) \leq 1400)$, the model predicted over 96% of the measured data in this mass flux range with $\pm 30\%$. These results are consistent with the results of Kim and Mudawar [11, 12] where a value of $n = 0.1$ was deemed suitable for *HTC* prediction in the Reynold number range of $10 \leq Re_l(\overline{u_l}, \delta) \leq 600$. For $n = 1.2$, the model predicted 100% of the measured heat transfer for $G \geq 200\ kg/(m^2s)$ within $\pm 20\%$ but under-predicted the measured heat transfer for $G \leq 100\ kg/(m^2s)$ particular for higher wall heat fluxes. The results suggest a dependence of n on both mass flux and heat flux.

We first examine the effect of mass flux on both n and the measured heat transfer coefficient. A high value of n, signifies significant turbulence damping close to the interface of the liquid film (i.e., smoother interface) [19]. According to Mudawar and El-Masri [19], the "*smooth-surface assumption can only be justified by the long waves* (roll waves) *that prevail in turbulent flows* (high Reynolds number flows)". In other words, with increase in the Reynolds number (or mass flux); the roll waves become dominant, the interface becomes smoother (free from ripples) and consequently n increases. In the current work, as Reynolds number of the liquid (or mass flux) increased so did the mean value of n that provided best prediction of the measured heat transfer coefficient in the current work. This agrees with the significance of n as described by Mudawar and El-Masri [19]. Over the range of vapor qualities, the average of the optimal values of n that gave best predictions of heat transfer coefficient in upward flow were $0.60, 0.74, 1.09$, and 1.27, for

$G = 75\,kg/(m^2s)$ $(700 \leq Re_l(\overline{u_l}, \delta) \leq 1000), G = 100\,kg/(m^2s)$ $(800 \leq Re_l(\overline{u_l}, \delta) \leq 1400), G = 200\,kg/(m^2s)$ $(1700 \leq Re_l(\overline{u_l}, \delta) \leq 3000)$ and $G = 400\,kg/(m^2s)$ $(4600 \leq Re_l(\overline{u_l}, \delta) \leq 6500)$, respectively.

Next, we examine the effect of heat flux on both n and the measured heat transfer coefficient at constant mass flux and vapour quality. While increase in mass flux increased the dominance of roll waves over ripples (i.e., increase in n), increase in heat flux produced the opposite effect. For $G \leq 200\ kg/(m^2s)$, there was significant amount of bubble nucleation in the annular film which detaches from the wall and coalesce with the interface resulting in increased interfacial disturbances and reduced interfacial damping. The density and frequency of detachment of nucleated bubbles in the annular film increases with wall heat flux resulting in higher interfacial disturbances (and reduced interfacial damping or n) with increase in heat flux. In the current work, the increased interfacial disturbances with increase in heat flux was deduced from the increase in both the interfacial shear stress and frequency of ripples with increase in heat flux [17]. Flow visualizations showing bubble nucleation in the annular film as well as that showing the effect of heat flux on interfacial shear stress and wave frequency have been provided in Ayegba et al. [17]. The eddy viscosity (Eqs. (40) and (41)) increase with the wall and interfacial shear stresses (

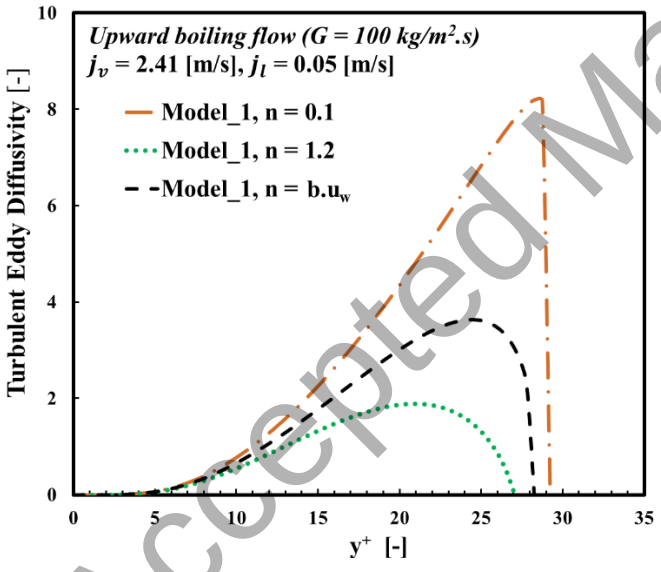

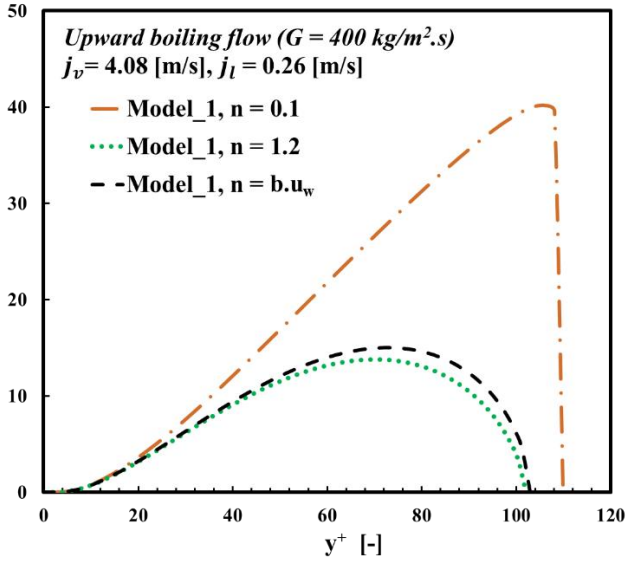

Figure 5) and as reported in various studies [10, 11, 19, 25, 33], the heat transfer coefficient increases with the interfacial shear stresses. This, again, is consistent with decrease in the optimal values of n (the value of n that best prediction of the measured heat transfer coefficient) with increase in heat flux.

In general, the optimal value of n was not constant but rather increased with mass flux and decreased with heat flux. The physical significant of n is seen as the modification of the interfacial shear stress by the interfacial structures. It should be remarked that changes in values of n had very limited effect on the computed liquid film thickness (δ).

As described above, the damping at the interface is linked to wave structures at the interface [19]. With increase in vapor Reynolds number, velocity fluctuations close the interface become increasingly dominated by inertia forces leading to increased viscous effects in the liquid sublayer close to the interface [19]. This creates a free-surface boundary layer with a liquid sublayer similar to that in the near-wall-region [19]. In the current work, the wave structure at the interface has been characterized by image processing of high-speed visualizations of the flow [17]. The roll waves velocities have been determined from space-time plots of the grey levels along an axial line (tube

center) of the image (Figure 9). Roll waves and ripples can be seen on this figure. At low value of *G* the ripples were clearly visible, but disappeared at higher values of *G* in agreement with the observations of Mudawar and El-Masri [19] An increase in total mass flux led to an increase in the measured mean velocity of roll waves (Figure 10(a)). On the other hand, with increase in heat flux, there was increase in bubble nucleation at the wall resulting in increased bubble coalescence with the interface as well as increased generation of ripples (Figure 9). This results in increased disturbance or mixing in the interfacial sublayer (decrease in interfacial damping) as well as reduced viscous effect in this layer. In the current work, both the measured mean velocity of roll waves and the optimal values of n for the prediction of heat transfer coefficient increased with mass flux and decreased with heat flux (Figure 10(a)). In other words, the optimal values of n for the prediction of heat transfer coefficient and the measured velocity of roll waves showed similar dependence on mass flux and heat flux. However, while the optimal values of n was generally independent of the vapour quality, the measured mean wave frequency increased with vapor quality. For this reason, a plot of optimal values of n versus measured mean velocity of roll waves did not show a clear pattern and therefore was not shown. Notwithstanding, in this work, an attempt was made to link the value of n to the wave velocity (u_w).

According to Sawant et al. [34], if the wave velocity is correlated against the modified Weber number (Eq. (53)), the wave velocity becomes independent of the Reynolds number of the liquid. A simple correlation for wave velocity is proposed in this work (Eq. (54)). The correlation predicted around 92% of the measured wave velocity within ± 20 (Figure 10(b)). A simple expression relating n to u_w was also proposed in this work (Eq. (54)). Similar to roll wave velocity, the value of n given by Eq. (55) increases with mass flux and vapor quality and also decreased with heat flux.

$$We_m = \frac{\rho_c j_v^2 D}{\sigma}\left(\frac{\rho_l - \rho_c}{\rho_c}\right)^{1/3} \tag{53}$$

$$u_w = \frac{2.18We_m}{55 + 1.14e5 \times Bo + We_m} \tag{54}$$

$$n = b.u_w \qquad b = \begin{cases} 0.60 & upward\ flow \\ 0.40 & downward\ flow \end{cases} \tag{55}$$

The value of n given by Eq. (55) was used in Eq. (41) and the procedure outlined in Figure 4 was followed to determine the various parameters of interest. Predicted velocity and temperature profiles in the liquid at selected conditions are shown in Figure 6 above along with profiles obtained for $n = 0.1$ and $n = 1.2$. The predicted heat transfer coefficient obtained for n given by Eq. (55) in upward flow is shown in Figure 11. The model predicted around 98% of the measured heat transfer within $\pm 20\%$ for the range of mass and heat fluxes tested. It is important to note that 98% the values of the film thickness calculated to match the liquid mass flux (Eq. (42)) is a good agreement (within $\pm 20\%$) with the measured values as shown in **Error! Reference source not found.**(a).

Heat transfer coefficient in downward flow

In downward flow, the interfacial shear stress is much lower relative to upward flow resulting in lower frequency of roll waves. The implication of this is lower interfacial damping, greater disturbances at the interface due to bubble coalescence with the interface and higher sensitivity of the interfacial shear stress to changes in heat flux. For similar conditions of flow, the optimal value of n in downward flow was significantly smaller relative to upward flow. Over the range of vapor qualities, the average of the optimal values of n that gave best predictions of heat transfer coefficient in downward flow were $0.29, 0.74, 0.75,$ and 1.21, for $G = 75\,kg/(m^2 s)$ $(700 \leq Re_l(\overline{u_l}, \delta) \leq 1000), G = 100\,kg/(m^2 s)$ $(800 \leq Re_l(\overline{u_l}, \delta) \leq 1400), G = 200\,kg/(m^2 s)$ $(1700 \leq Re_l(\overline{u_l}, \delta) \leq 3000)$ and $G = 400\,kg/(m^2 s)$ $(4600 \leq Re_l(\overline{u_l}, \delta) \leq 6500)$, respectively. In general, the optimal value of n was not constant but rather increased with mass flux and vapour quality but decreased with heat flux. It should be remarked that in the current work, the change in flow direction had only limited effect on the wave velocity and Eq. (52) predicted around 92% of the measured wave velocity in downward flow within $\pm 20\%$. The effect of change in flow direction from upward to downward flow was more obvious in the change in wave frequency and was higher in the former. For the case of downward flow, the expression for n given by Eq. (55) provided the best predictions of the measured heat transfer

coefficient.

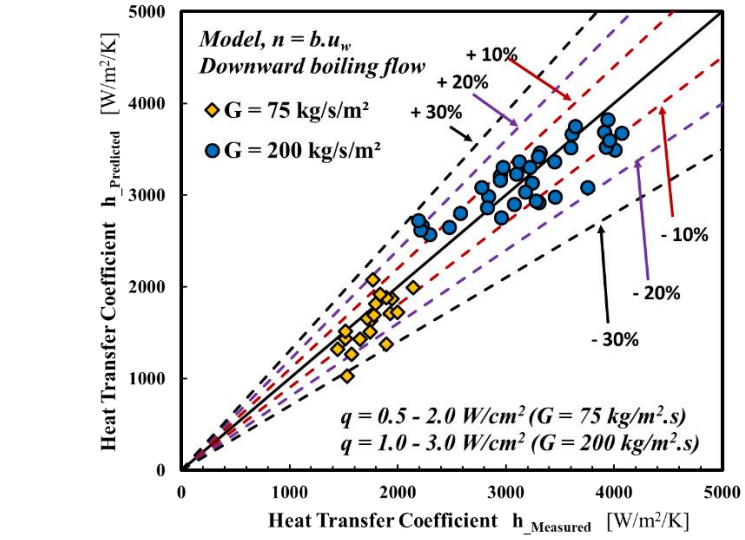

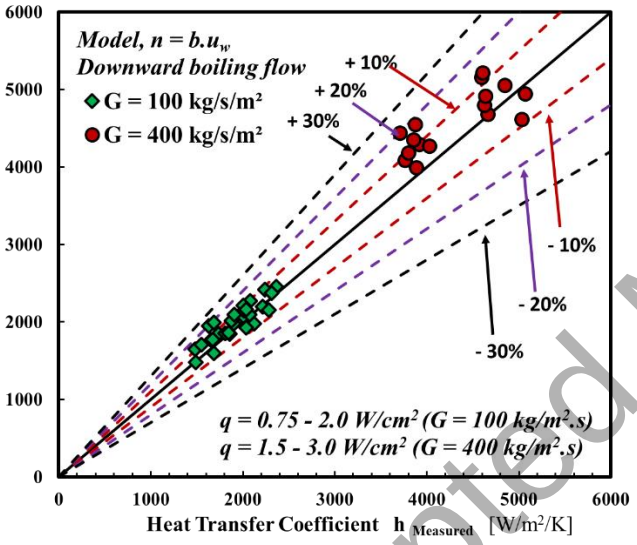

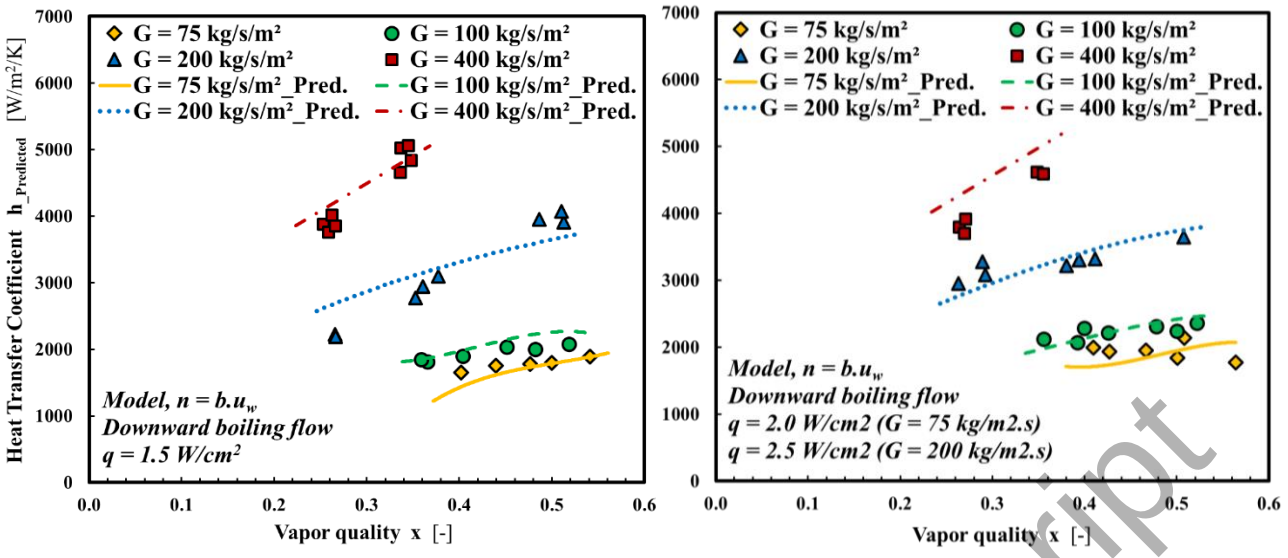

Figure *13* shows measured and predicted heat transfer for n given by Eq. (55). The model predicted over 96% of the experimental data within $\pm 20\%$ for the range of mass and heat flux tested. Furthermore, it provided a better representation of the trends in the measured data.

Liquid film thickness in upward and downward flows

In line with the solution scheme in Figure 4, the predicted liquid film thickness corresponds to the liquid film thickness for which there is mass conservation in the liquid film. In the current work, liquid film thickness was estimated from measured void fraction. The uncertainty in measured liquid film thickness is provided in [17]. **Error! Reference source not found.** provides a comparison between measured and predicted liquid film thickness in upward and downward flows, with some error bars to give an estimation of the measurement accuracy. The models predicted around 98% of the measured film thickness in upward (within $\pm 20\%$) and downward (within $\pm 30\%$) flows. The slight over-prediction in downward flow for $G \leq 100\, kg/m^2 s$ is due to the fact that, the experimental liquid film thickness under these conditions was very thin (relative to upward flow) [17]. In the current work, the experimental measurement uncertainties of the liquid film thickness for thin liquid films (high void fraction) were high ($\Delta\delta/\delta \approx 45\%$ for $x \geq 0.35$) [17]. It

should be remarked that changes in n from 0.1 to 1.2 had very limited effect on the predicted liquid film thickness (Figure 14).

Conclusions

Eddy-diffusivity-based theoretical models for predicting heat transfer coefficient in upward and downward flow boiling were developed in this work. The models were developed using heat-flux-dependent wall shear stress correlations and the interfacial damping function was modelled using wave structures. Some of the important findings include:

1. The proposed models predicted over 96% of the measured heat transfer coefficient within $\pm 20\%$ in both upward and downward flows and also reproduced the heat flux dependence of the measured heat transfer coefficient. The heat flux dependence was particular important for $Re_l < 4000$ where nucleation was present in the annular liquid film [17].
2. The proposed models predicted over 96% of the measured liquid film thickness within $\pm 30\%$ in both upward and downward flows. This was within the range of experimental uncertainty of the measured film thickness.
3. It was found that interfacial damping depends on the Reynolds number of the liquid film. A first attempt towards improving the interfacial damping function originally proposed by Mudawar and El-Masri [19] was carried out. The determination of optimal values of the exponent (n) of the interfacial damping function from roll wave velocity improved model predictions from within $\pm 30\%$ to within $\pm 20\%$.

4. The predicted dimensionless velocity and temperature profiles were higher than single phase flow and increased with n. These results generally agree with both experimental and modelling studies in literature (Ashwood et al. [32]; Chen et al. [25]; Kim and Mudawar [11]; Sun et al. [30]; Zadrazil and Markides [31]).

Nomenclature

A^+	constant
Bo	Boiling number
b	constant
C	constant
C_p	specific heat at constant pressure, J/(kgK)
D	Diameter, m
f	friction factor
G	mass flux, kg/(m^{2}s)
g	acceleration due to gravity, m/(s^2)
h	heat transfer coefficient or specific enthalpy, W/(m^{2}K) or J/(kgK)
$h_{l,v}$	latent heat of vaporization, J/kg
HTC	heat transfer coefficient, W/(m^{2}K)
ITO	indium-tin-oxide
j	mixture or superficial velocity, m/s
K	von Karman constant
k	thermal conductivity of sapphire tube, W/(mK)
L	length of the test section, m
l	mixing length, m
l^+	dimensionless mixing length
$\dot{m}$	mass flow rate, kg/s
n	exponent of the interfacial damping function
p	Pressure, bar

P Power, W

Pr Prandtl number

q heat flux, W/m^2

R Radius, m

R^+ dimensionless radius

Re Reynolds number

r radial coordinate, m

Su Suratman number

T Temperature, K

T^+ dimensionless temperature

t Time, s

u mean velocity, m/s

u^* friction velocity, m/s

$\overline{u_l}$ mean liquid velocity, m/s

We Weber number

X Martinelli or laminarization parameter

x vapor quality

y distance from the wall, m

y^+ dimensionless distance from the wall

y^* frictional distance from the wall, m

z axis coordinate, m

Greek symbols

α void fraction

δ liquid film thickness, m

δ^+ dimensionless liquid film thickness

ε_m eddy viscosity, m^2/s

ϕ Martinelli parameter

μ dynamic viscosity, Pa.s

ν kinematic viscosity, m^2/s

ρ Density, kg/m^3

σ surface tension and dielectric constant, N/m

τ shear stress, Pa

θ Inclination, degree

Subscripts

A adiabatic

c vapor core

eff effective

Exp experimental

fr frictional

i inner or interfacial

in inlet conditions

k phase

l liquid phase

lam laminar or laminarization

lo liquid only

m mixture or modified

NA non-adiabatic

o outer

ph preheater

pred predicted

sat saturated conditions

t turbulent or total

v vapor phase

vo liquid only

w wall or wave

∞ infinity

Acknowledgements

Petroleum Technology Development Fund (PTDF) is acknowledged for the PhD grant funding of P. Ayegba. The European Space Agency (ESA) and the French Space Agency (CNES) through the GDR 2799 Micropesanteur Fondamentale et Appliquée are acknowledged for the financial support in the building of the experimental set-up.

References

[1] Z. Liu and R.H.S. Winterton, "A general correlation for saturated and subcooled flow boiling in tubes and annuli, based on a nucleate pool boiling equation," *International Journal of Heat and Mass Transfer*, vol. 34, no. 11, pp. 2759–2766, 1991. DOI: 10.1016/0017-9310(91)90234-6.

[2] K.E. Gungor and R.H.S. Winterton, "A general correlation for flow boiling in tubes and annuli," *International Journal of Heat and Mass Transfer*, vol. 29, no. 3, pp. 351–358, 1986. DOI: 10.1016/0017-9310(86)90205-X.

[3] S.G. Kandlikar, "A general correlation for saturated two-phase flow boiling heat transfer inside horizontal and vertical tubes," *Journal of Heat Transfer*, vol. 112, no.1, pp. 219–228, 1990. DOI: 10.1115/1.2910348.

[4] S.-M. Kim and I. Mudawar, "Universal approach to predicting saturated flow boiling heat transfer in mini/micro-channels – Part II, Two-phase heat transfer coefficient," *International Journal of Heat and Mass Transfer*, vol. 64, pp. 1239–1256, Sept. 2013. DOI: 10.1016/j.ijheatmasstransfer.2013.04.014.

[5] D. Mikielewicz and J. Mikielewicz, "A common method for calculation of flow boiling and flow condensation heat transfer coefficients in minichannels with account of nonadiabatic effects," *Heat Transfer Engineering*, vol. 32, no. 13-14, pp. 1173–1181, 2011. DOI: 10.1080/01457632.2011.562728.

[6] H. Wang and X. Fang, "Evaluation analysis of correlations of flow boiling heat transfer coefficients applied to ammonia," *Heat Transfer Engineering*, vol. 37, no.1, pp. 32–44, 2016. DOI: 10.1080/01457632.2015.1025006.

[7] O.E. Turgut, H. Genceli, M. Asker, and M.T. Çoban, "Novel saturated flow boiling correlations for R600a and R717 refrigerants," *Heat Transfer Engineering*, vol. 43, no. 18, pp. 1579-1609, 2022. DOI: 10.1080/01457632.2021.1989843.

[8] A. Cioncolini, J.R. Thome, and C. Lombardi, "Algebraic turbulence modeling in adiabatic gas-liquid annular two-phase flow," *International Journal of Multiphase Flow*, vol. 35, no.6 pp. 580–596, 2009. DOI: 10.1016/j.ijmultiphaseflow.2009.02.002.

[9] A. Cioncolini and J.R. Thome, "Algebraic turbulence modeling in adiabatic and evaporating annular two-phase flow," *International Journal of Heat and Fluid Flow*, vol. 32, no. 4, pp. 805–817, 2011. DOI: 10.1016/j.ijheatfluidflow.2011.05.006.

[10] H. Ohta, "Microgravity heat transfer in flow boiling," in *Advances in Heat Transfer*, vol. 37, 1st ed., J.P. Hartnett, T.F. Irvine, Y.I. Cho and G.A. Greene, Eds. California, USA: Elsevier, 2003, pp. 1–75.

[11] S.-M. Kim and I. Mudawar, "Theoretical model for local heat transfer coefficient for annular flow boiling in circular mini/micro-channels," *International Journal of Heat and Mass Transfer*, vol. 73, pp. 731–742, Jun. 2014. DOI: 10.1016/j.ijheatmasstransfer.2014.02.055.

[12] S.-M. Kim and I. Mudawar, "Theoretical model for annular flow condensation in rectangular micro-channels," *International Journal of Heat and Mass Transfer*, vol. 55, no. 4, pp. 958–970, 2012. DOI: 10.1016/j.ijheatmasstransfer.2011.10.014.

[13] A. Cioncolini and J.R. Thome, "Pressure drop prediction in annular two-phase flow in macroscale tubes and channels," *International Journal of Multiphase Flow*, vol. 89, pp. 321–330, Mar. 2017. DOI: 10.1016/j.ijmultiphaseflow.2016.11.003.

[14] S.-M. Kim and I. Mudawar, "Review of databases and predictive methods for pressure drop in adiabatic, condensing and boiling mini/micro-channel flows," *International Journal of Heat and Mass Transfer*, vol. 77, pp. 74–97, Oct. 2014. DOI: 10.1016/j.ijheatmasstransfer.2014.04.035.

[15] T. Layssac, "Contribution à l'étude phénoménologique de l'ébullition convective en mini-canal," Ph.D. thesis, Université de Lyon, Lyon, France, 2018.

[16] S.-M. Kim and I. Mudawar, "Universal approach to predicting two-phase frictional pressure drop for mini/micro-channel saturated flow boiling," *International Journal of Heat and Mass Transfer*, vol. 58, no. 1-2, pp. 718–734, 2013. DOI: 10.1016/j.ijheatmasstransfer.2012.11.045.

[17] P.O. Ayegba, J. Sebilleau, and C. Colin, "Hydrodynamics of vertical upward and downward flow boiling in a millimetric tube," *International Journal of Multiphase Flow*, vol. 153, pp. 104120, Aug.2022. DOI: 10.1016/j.ijmultiphaseflow.2022.104120.

[18] C.B. Tibiriçá, G. Ribatski, and C.B. Tibiriçtibiriç, "Two-phase frictional pressure drop and flow boiling heat transfer for R245fa in a 2.32-mm tube," *Heat Transfer Engineering*, vol. 32, no. 13-14, pp. 1139–1149, 2011. DOI: 10.1080/01457632.2011.562725.

[19] I.A. Mudawar and M.A. El-Masri, "Momentum and heat transfer across freely-falling turbulent liquid films," *International Journal of Multiphase Flow*, vol. 12, no. 5, pp. 771–790, 1986. DOI: 10.1016/0301-9322(86)90051-0.

[20] E.R. van Driest, "On turbulent flow near a wall," *Journal of the Aeronautical Sciences*, vol. 23, no. 11, pp. 1007–1011, Nov. 1956. DOI: 10.2514/8.3713.

[21] W.M. Kays, "Heat transfer to the transpired turbulent boundary layer," *International Journal of Heat and Mass Transfer*, vol. 15, no. 5, pp. 1023–1044, 1972. DOI: 10.1016/0017-9310(72)90237-2.

[22] W.M. Kays and M.E. Crawford, *Convective Heat and Mass Transfer*, 3rd ed. New York, NY, USA: McGraw-Hill, 1980.

[23] S. Lee and I. Mudawar, "Enhanced model for annular flow in micro-channel heat sinks, including effects of droplet entrainment/deposition and core turbulence," *International Journal of Heat and Mass Transfer*, vol. 133, pp. 510–530, Apr. 2019. DOI: 10.1016/j.ijheatmasstransfer.2018.12.074.

[24] S.-M. Kim and I. Mudawar, "Theoretical model for local heat transfer coefficient for annular flow boiling in circular mini/micro-channels," *International Journal of Heat and Mass Transfer*, vol. 73, pp. 731–742, Jun. 2014. DOI: 10.1016/j.ijheatmasstransfer.2014.02.055.

[25] C. Chen *et al*., "Theoretical calculation of the characteristics of annular flow in a rectangular narrow channel," *Annals of Nuclear Energy*, vol. 85, pp. 259–270, Nov. 2015. DOI: 10.1016/j.anucene.2015.05.027.

[26] M. Narcy, E. de Malmazet, and C. Colin, "Flow boiling in tube under normal gravity and microgravity conditions," *International Journal of Multiphase Flow*, vol. 60, pp. 50–63, Apr. 2014. DOI: 10.1016/j.ijmultiphaseflow.2013.11.011.

[27] A. Cioncolini, J.R. Thome, and C. Lombardi, "Unified macro-to-microscale method to predict two-phase frictional pressure drops of annular flows," *International Journal of Multiphase Flow*, vol. 35, no. 12, pp. 1138–1148, 2009. DOI: 10.1016/j.ijmultiphaseflow.2009.07.005.

[28] G.F. Hewitt and N.S. Hall-Taylor, *Annular Two-Phase Flow*, 1st ed. Oxford, UK: Pergamon Press Ltd., 1970.

[29] S.-M. Kim and I. Mudawar, "Universal approach to predicting two-phase frictional pressure drop for adiabatic and condensing mini/micro-channel flows," *International Journal of Heat and Mass Transfer*, vol. 55, no. 11-12, pp. 3246–3261, 2012. DOI: 10.1016/j.ijheatmasstransfer.2012.02.047.

[30] S. Sun, Y. Wu, and R. Zhao, "The numerical calculation of heat transfer performance for annular flow of liquid nitrogen in a vertical annular channel," *Cryogenics*, vol. 41, no.4, pp. 231–237, 2001. DOI: 10.1016/S0011-2275(01)00058-3.

[31] I. Zadrazil and C.N. Markides, "An experimental characterization of liquid films in downwards co-current gas-liquid annular flow by particle image and tracking velocimetry," *International Journal of Multiphase Flow*, vol. 67, pp. 42–53, Dec. 2014. DOI: 10.1016/j.ijmultiphaseflow.2014.08.007.

[32] A.C. Ashwood *et al.*, "A multiphase, micro-scale PIV measurement technique for liquid film velocity measurements in annular two-phase flow," *International Journal of Multiphase Flow*, vol. 68, pp. 27–39, Jan. 2015. DOI: 10.1016/j.ijmultiphaseflow.2014.09.003.

[33] F. Fu and J.F. Klausner, "A separated flow model for predicting two-phase pressure drop and evaporative heat transfer for vertical annular flow," *International Journal of Heat and Fluid Flow*, vol. 18, no. 6, pp 541–549, 1997. DOI: 10.1016/S0142-727X(97)00001-5.

[34] P. Sawant, M. Ishii, T. Hazuku, T. Takamasa, and M. Mori, “Properties of disturbance waves in vertical annular two-phase flow,” *Nuclear Engineering and Design*, vol. 238, no. 12, pp. 3528–3541, 2008. DOI: 10.1016/j.nucengdes.2008.06.013.

List of Figure Captions

flow, (c) and (d) measured and predicted heat transfer coefficient versus vapor quality in upward flow.

Figure 12. Predicted versus measured film thickness in the annular flow regime, (a) upward flow and (b) downward flow.

Figure 13. (a) and (b) predicted heat transfer coefficient versus measured heat transfer in downward flow, (c) and (d) measured and predicted heat transfer coefficient versus vapor quality in downward flow.

Figure 14. Predicted versus measured film thickness in the annular flow regime, (a) and (b) upward flow, (c) and (d) downward flow. (a) and (c) n=0.1, (b) and (d) n=1.2.

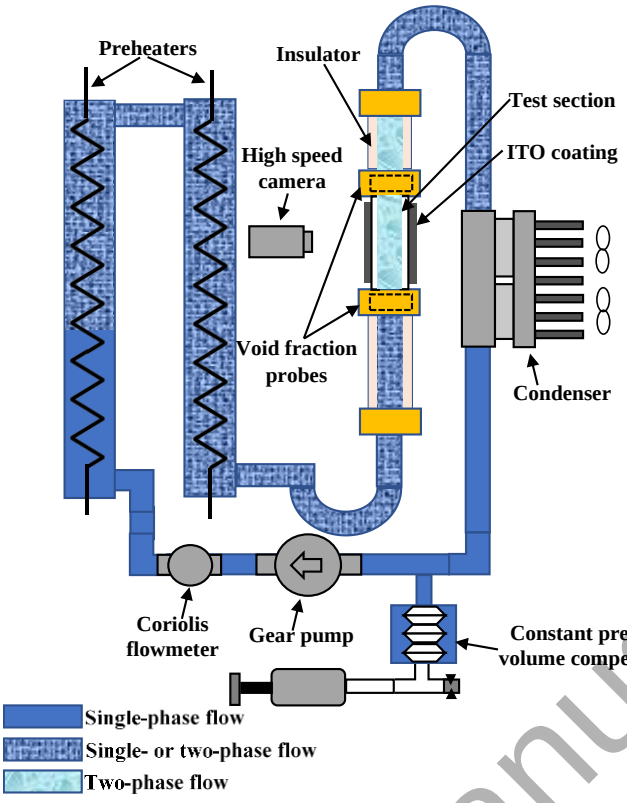

Figure 1. Experimental set-up (adapted from [17]).

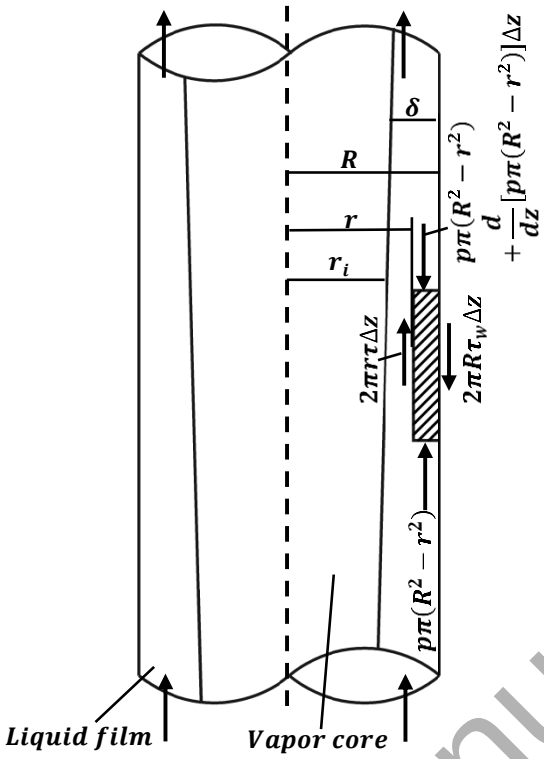

Figure 2. Control volume analysis in the liquid film of annular flow.

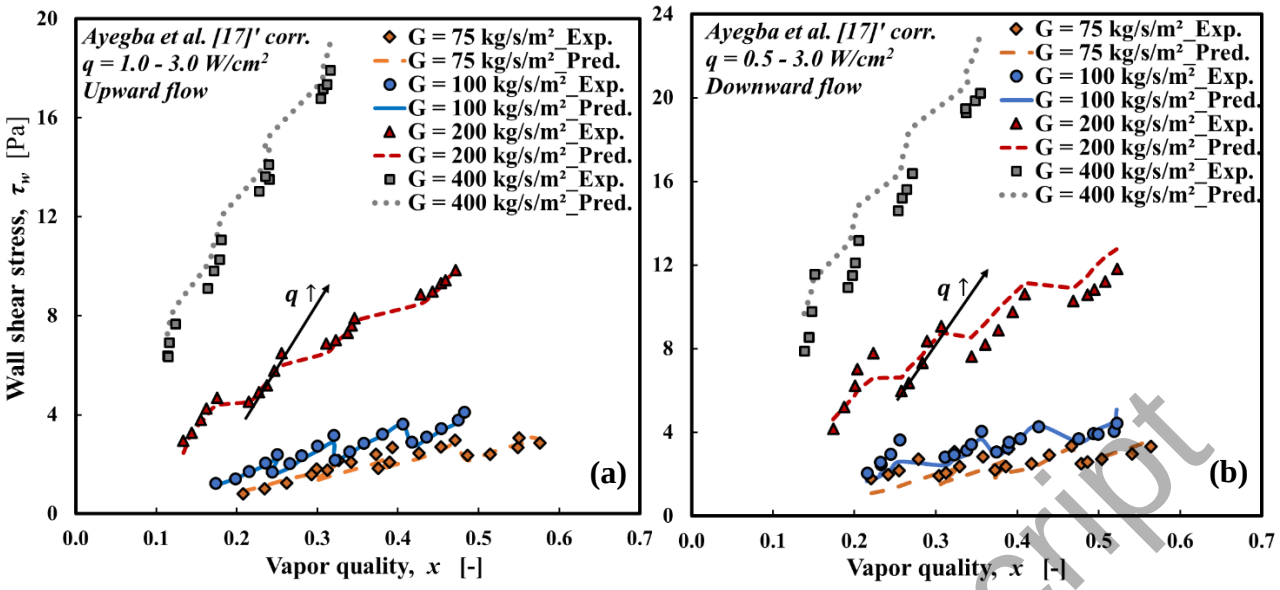

Figure 3. Wall shear stress versus quality for (a) upward and (b) downward annular flows; measured data (symbols), correlation of Ayegba et al. [17] (lines).

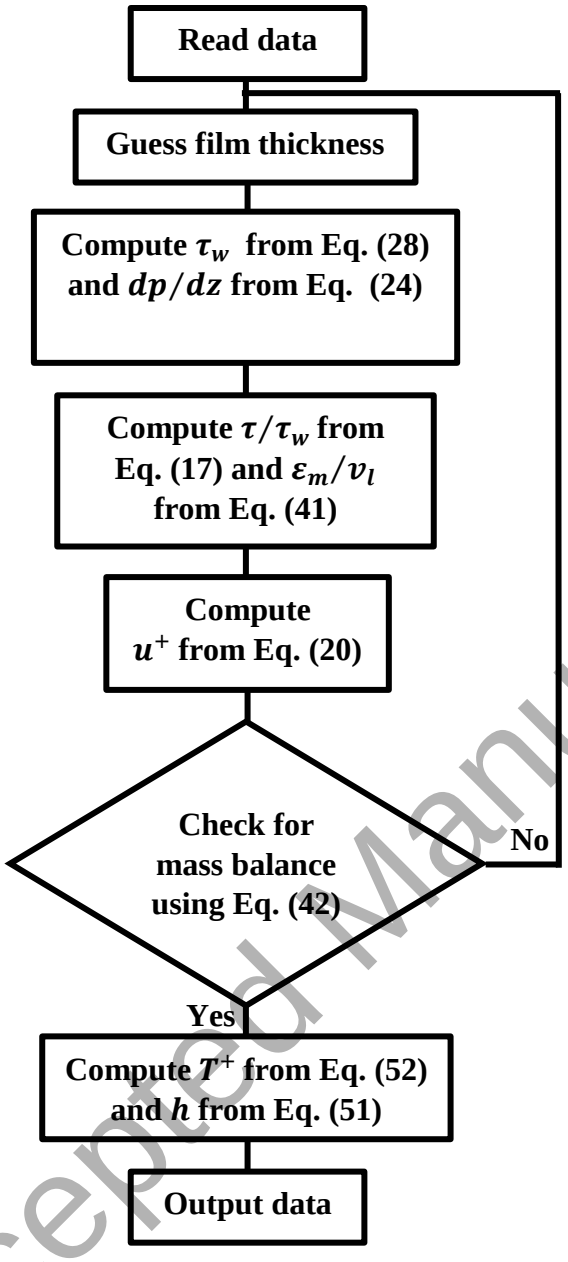

Figure 4. Numerical solution scheme.

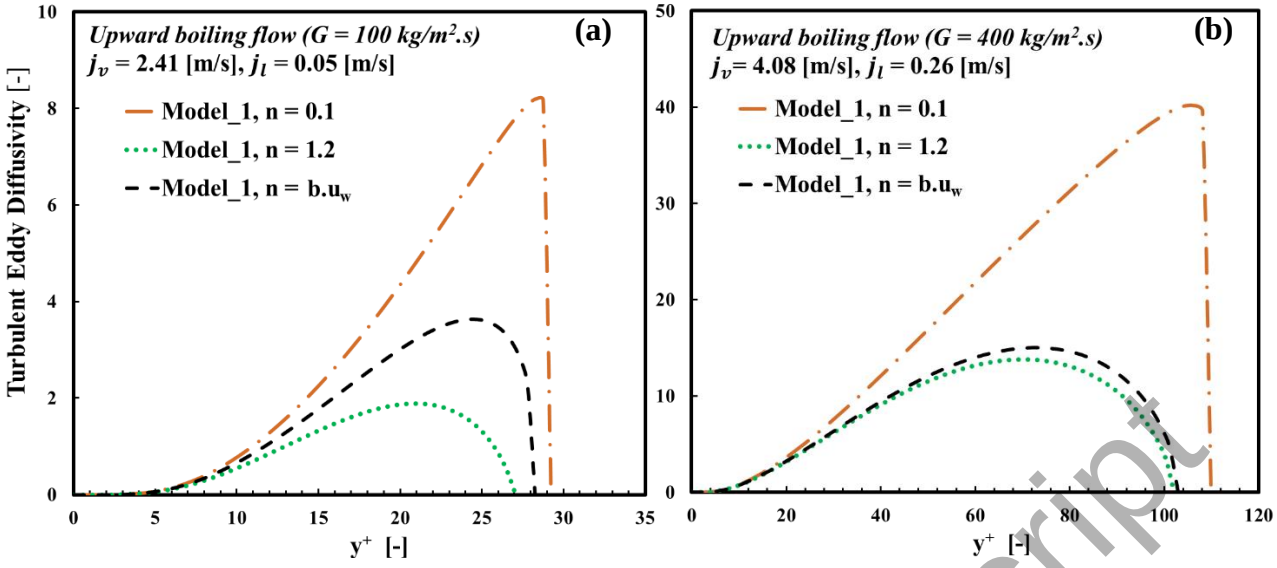

Figure 5. Eddy viscosity versus dimensionless distance from the wall in upward flow. (a) $G = 100\ kg/(m^2 s)$, (b) $G = 400\ kg/(m^2 s)$.

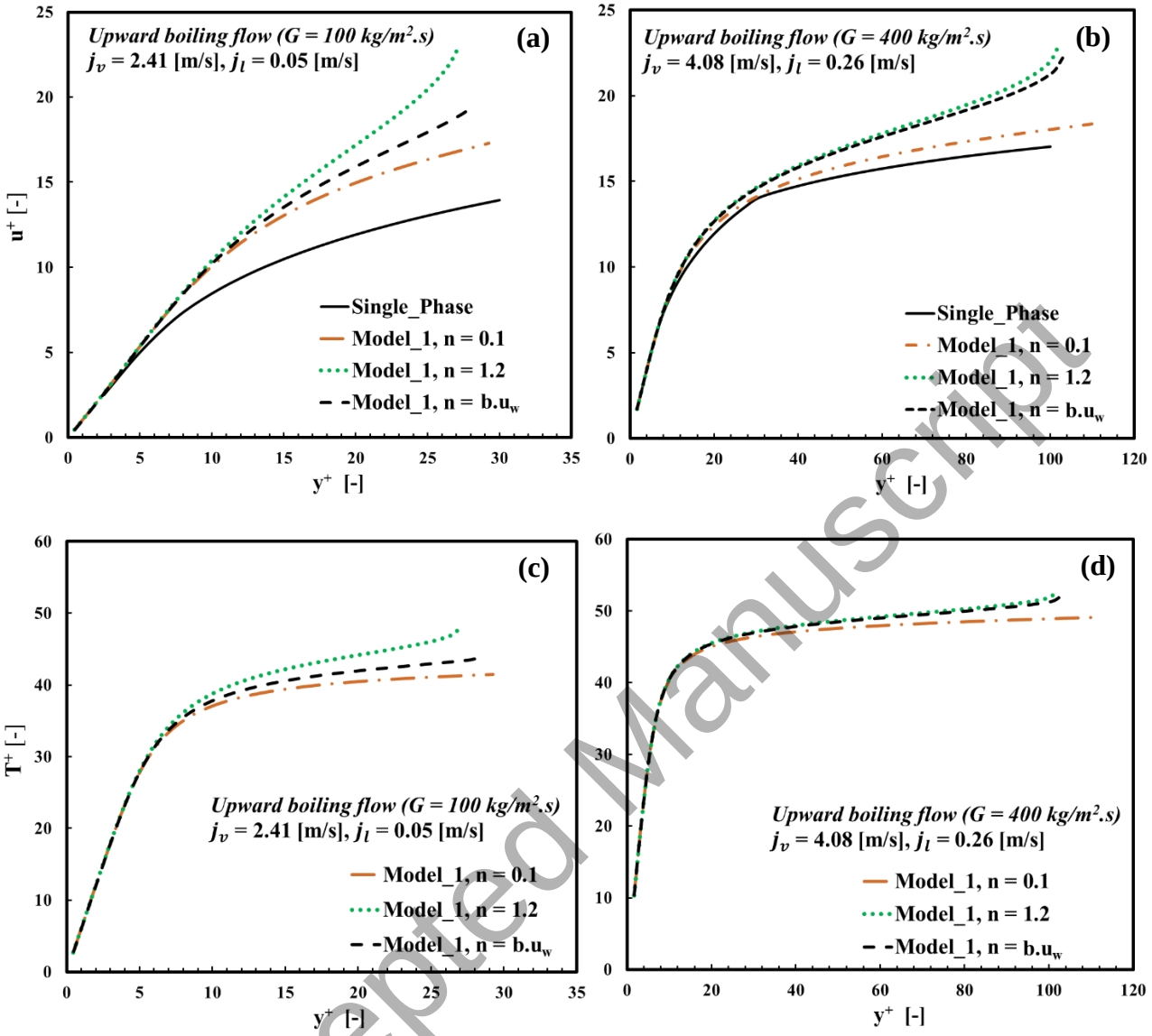

Figure 6. (a) and (b) dimensionless velocity profile versus dimensionless distance from the wall in upward flow, (c) and (d) dimensionless temperature profiles versus dimensionless distance from the wall in upward flow.

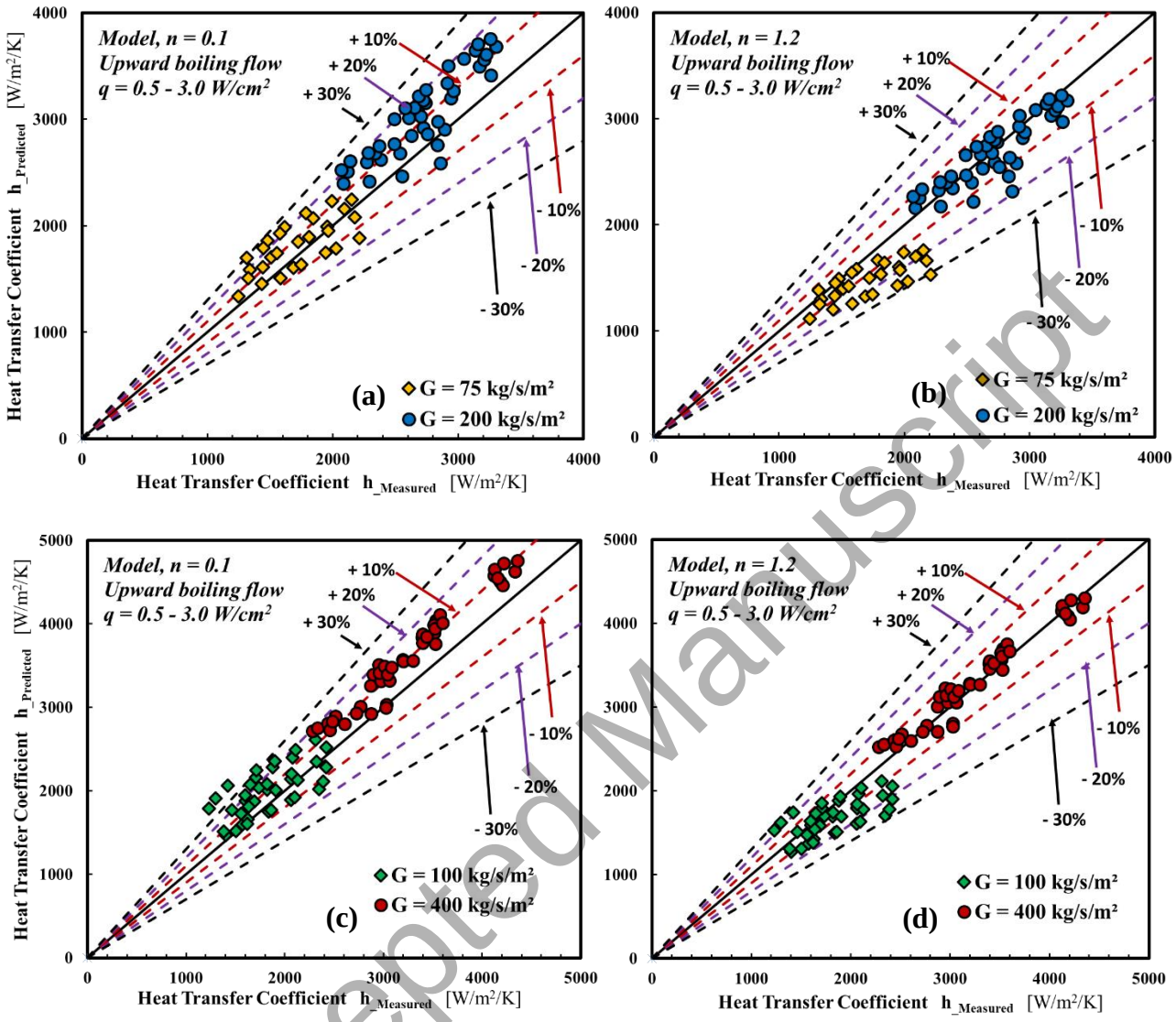

Figure 7. Predicted heat transfer versus measured heat transfer in upward flow, (a) and (c) $n = 0.1$ (b) and (d) $n = 1.2$.

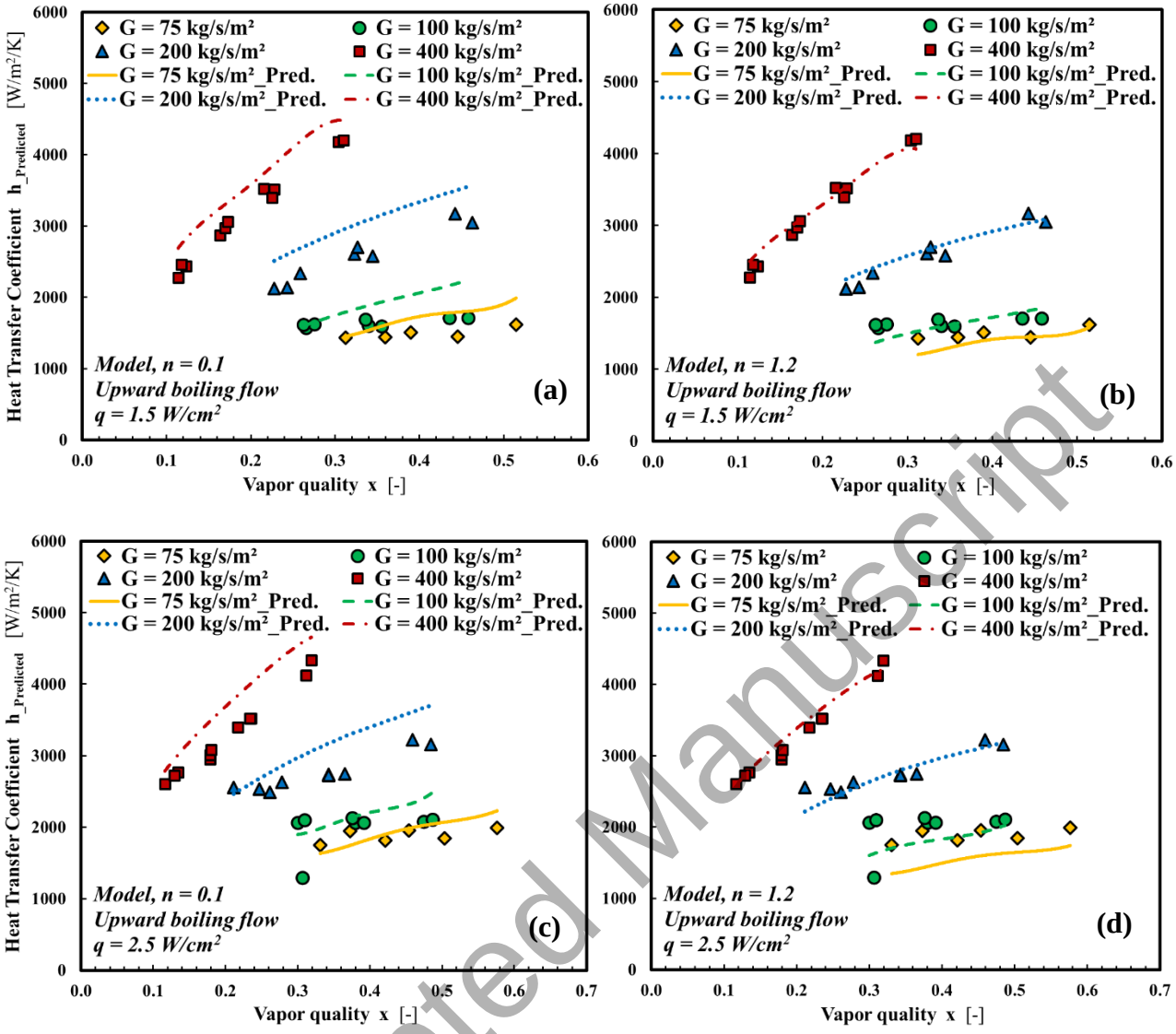

Figure 8. Measured and predicted heat transfer versus vapor quality in upward flow, (a) and (c) $n = 0.1$ (b) and (d) $n = 1.2$.

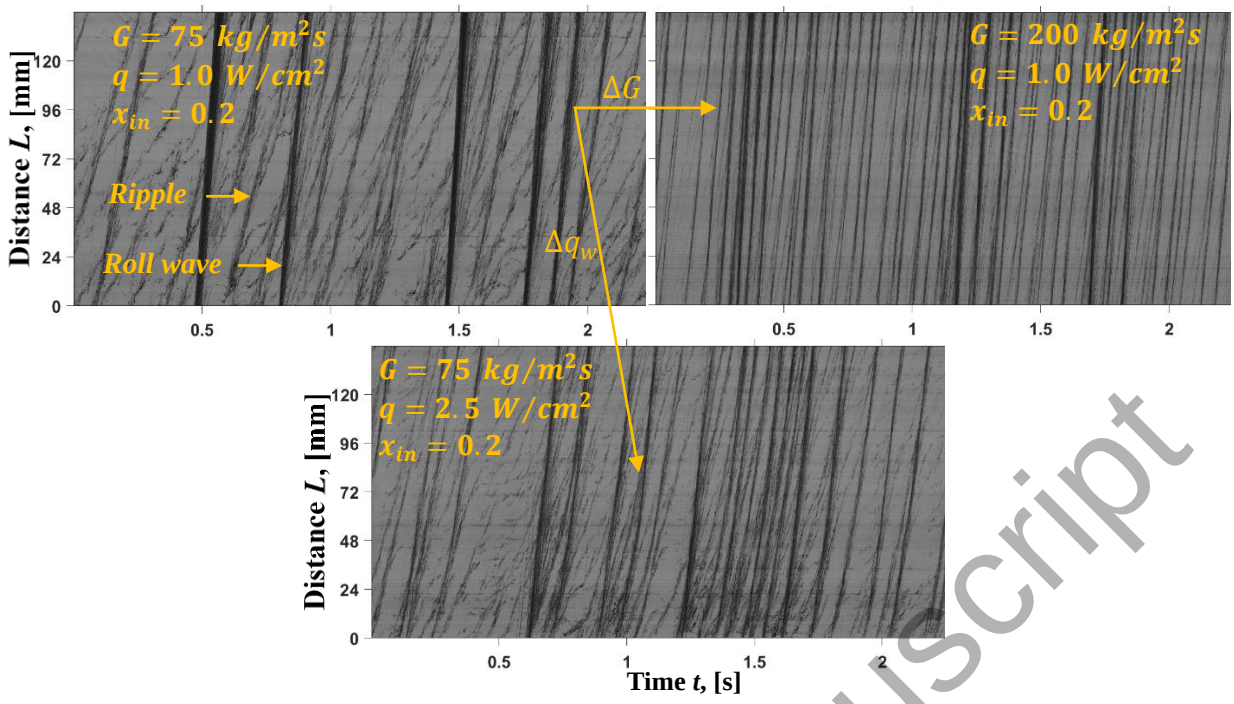

Figure 9. Time-space plot of the grey levels in the tube center line.

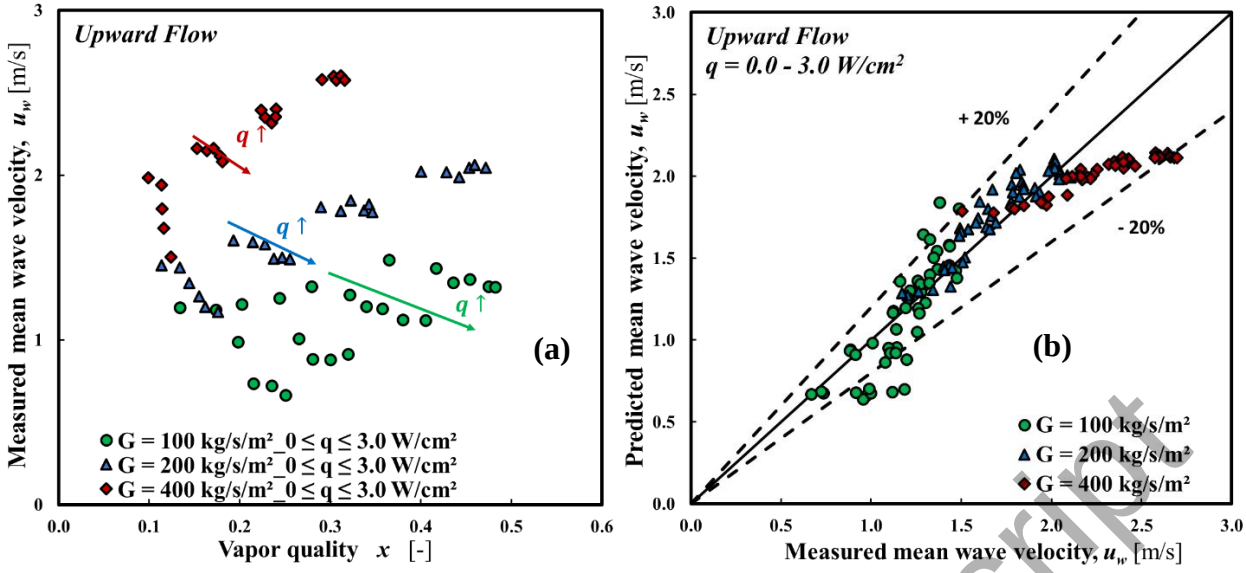

Figure 10. (a) measured mean roll wave velocity versus vapor quality and (b) predicted (Eq. (54)) versus measured mean roll wave velocity.

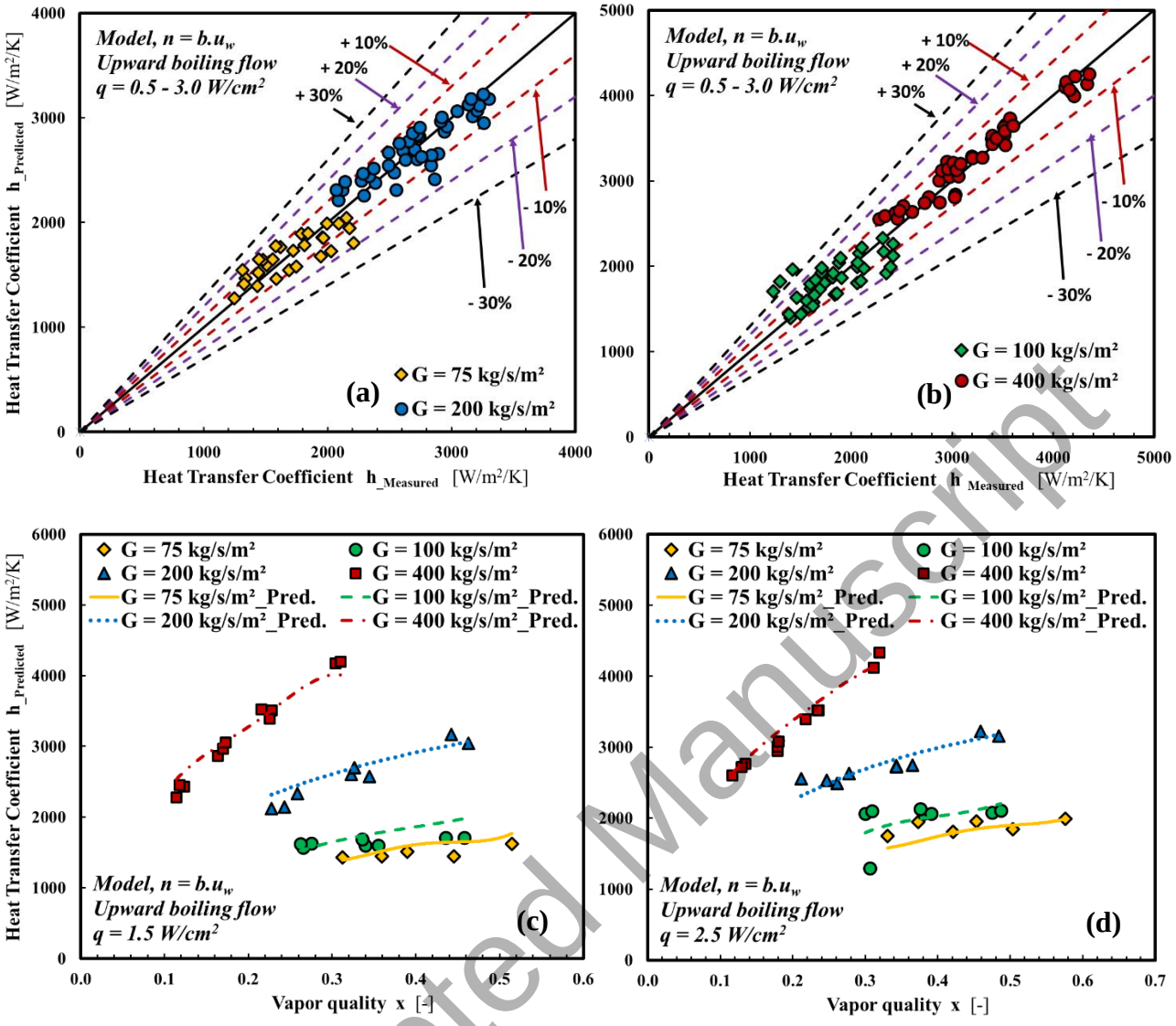

Figure 11. (a) and (b) predicted heat transfer coefficient versus measured heat transfer in upward flow, (c) and (d) measured and predicted heat transfer coefficient versus vapor quality in upward flow.

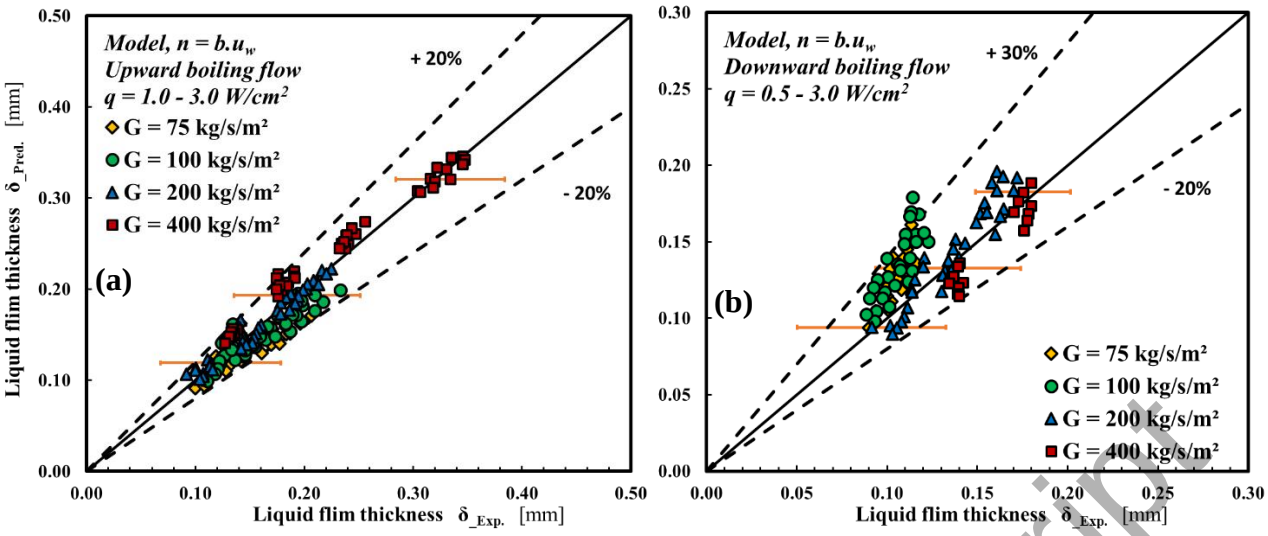

Figure 12. Predicted versus measured film thickness in the annular flow regime, (a) upward flow and (b) downward flow.

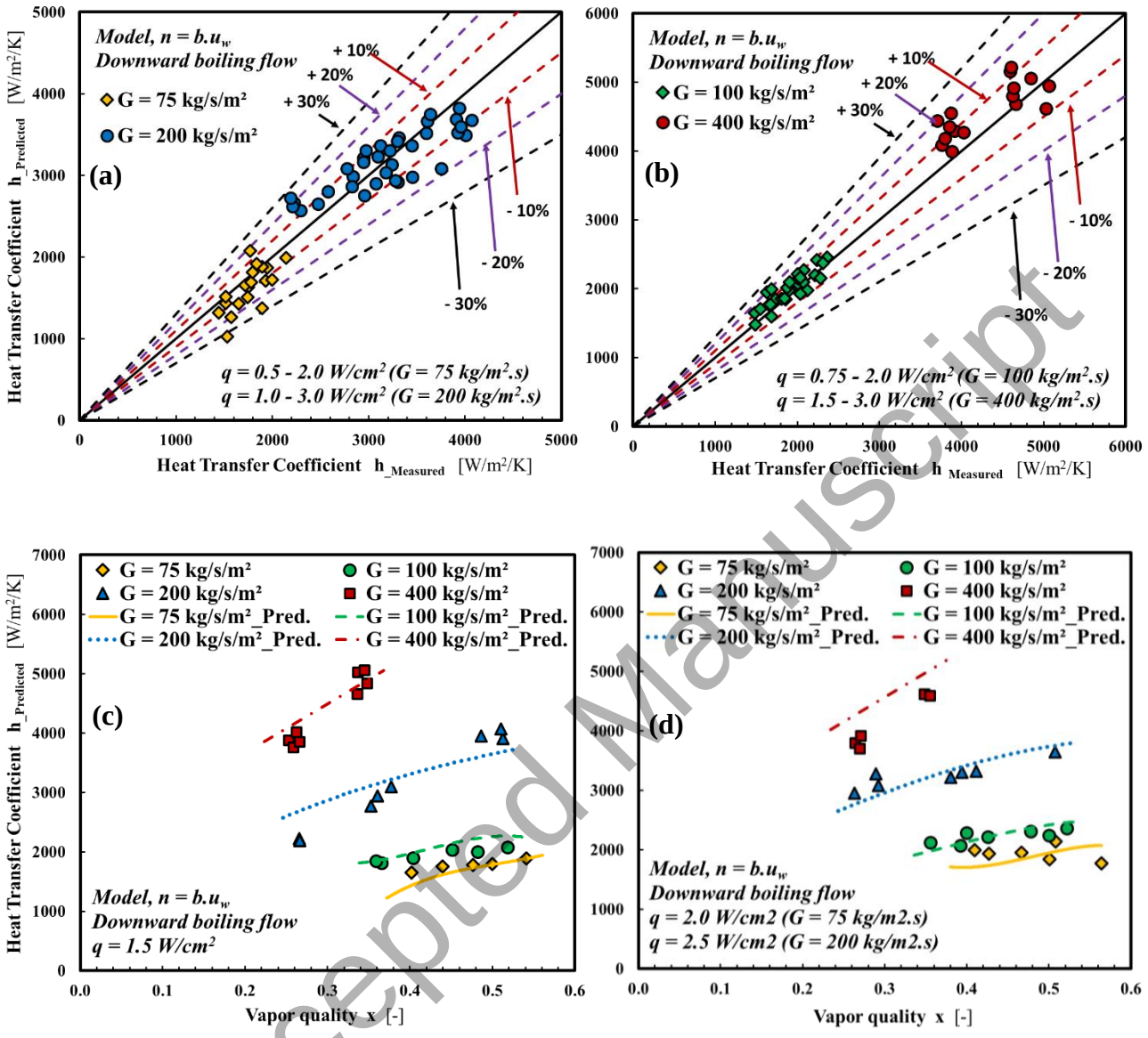

Figure 13. (a) and (b) predicted heat transfer coefficient versus measured heat transfer in downward flow, (c) and (d) measured and predicted heat transfer coefficient versus vapor quality in downward flow.

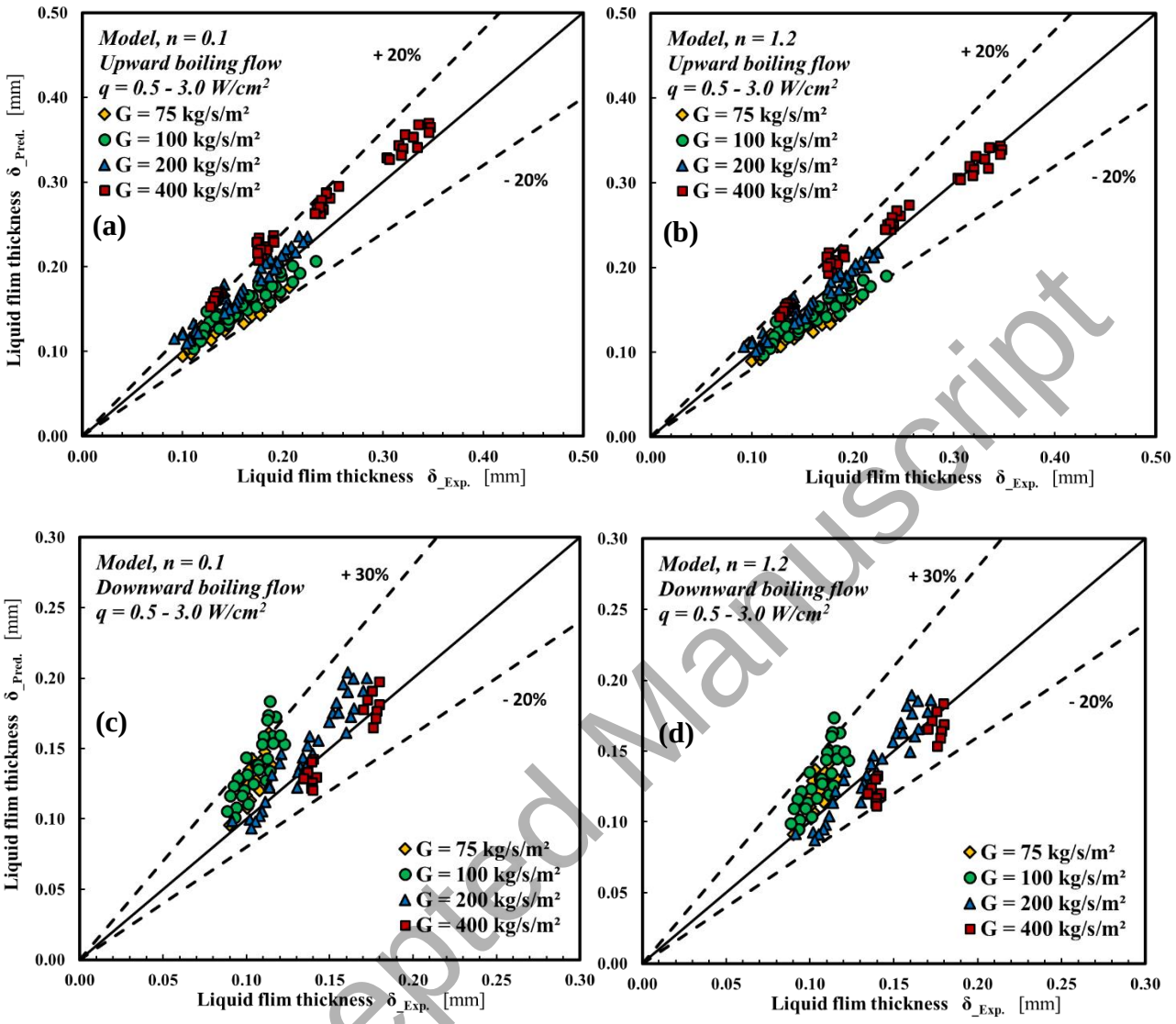

Figure 14. Predicted versus measured film thickness in the annular flow regime, (a) and (b) upward flow, (c) and (d) downward flow. (a) and (c) $n = 0.1$, (b) and (d) $n = 1.2$.

Notes on contributors

Paul O. Ayegba is a PhD student at Institut National Polytechnique de Toulouse, France/ Institut de Mécanique des Fluides de Toulouse, France. His PhD subject is in fluid mechanics. He was a recipient of the J.W. Fulbright Visiting Scholar Grant at the University of California Berkeley (2018-2019) and a recipient of the Petroleum Technology Development Fund (PTDF) PhD Scholarship (2019-2022). He has a good academic research profile with over 10 publications as well as field work experience.

Julien Sebilleau is an Assistant Professor at the University of Toulouse and Researcher at the Institute of Fluid Mechanics in Toulouse (IMFT). He obtained his PhD in 2009 in Paris and joined IMFT in 2011. His main research topics are two-phase flow in normal and microgravity conditions, phase change, wetting, and capillary flows. He is involved in several national and international networks and projects on two-phase flow for space applications and nuclear industry. He has authored 39 publications in peer reviewed journals or proceedings of international conferences.

Catherine Colin is a Professor at the University of Toulouse and Researcher at the Institute of Fluid Mechanics in Toulouse (IMFT). She obtained her PhD in 1990 in Toulouse and joined IMFT as CNRS researcher. She became full Professor in 2002. Her main research topics are two-phase flow in normal and microgravity conditions, bubble dynamics, breakup and coalescence, turbulence modelling, pool, and convective boiling. She is involved in several national and international networks and projects on two-phase flow for space applications and nuclear industry. She has authored 150 publications in

peer reviewed journals or proceedings of international conferences and 15 keynote lectures in international conferences. She was associate editor of Experimental Thermal and Fluid Science (2010-2018) and is associate editor of International Journal of Multiphase flows since 2018. She is involved in the scientific committees or co-chair of several international conferences (International Conference on Multiphase Flow, International Conference on Boiling and Condensation Heat Transfer, Experimental Heat Transfer Fluid Flow and Thermodynamics). She was Vice Chair in charge of research at the Polytechnic National Institute of Toulouse (2016-2020).